

This discussion paper is/has been under review for the journal Atmospheric Chemistry and Physics (ACP). Please refer to the corresponding final paper in ACP if available.

EPP impact on the middle atmosphere

K. Semeniuk et al.

Middle atmosphere response to the solar cycle in irradiance and ionizing particle precipitation

K. Semeniuk¹, V. I. Fomichev¹, J. C. McConnell¹, C. Fu², S. M. L. Melo², and I. G. Usoskin³

¹Department of Earth and Space Science and Engineering, York University, Toronto, Ontario, Canada

²Canadian Space Agency, St.-Hubert, Quebec, Canada

³Sodankylä Geophysical Laboratory, University of Oulu, Oulu, Finland

Received: 5 October 2010 – Accepted: 12 October 2010 – Published: 25 October 2010

Correspondence to: K. Semeniuk (kirill@nimbus.yorku.ca)

Published by Copernicus Publications on behalf of the European Geosciences Union.

Title Page	
Abstract	Introduction
Conclusions	References
Tables	Figures
◀	▶
◀	▶
Back	Close
Full Screen / Esc	
Printer-friendly Version	
Interactive Discussion	



Abstract

The impact of NO_x and HO_x production by three types of energetic particle precipitation (EPP), aurora, solar proton events and galactic cosmic rays is examined using a chemistry climate model. Ensemble simulations forced by transient EPP derived from observations with one-year repeating sea surface temperatures and fixed chemical boundary conditions were conducted for cases with and without solar cycle in irradiance. Our model results show a wintertime polar stratosphere ozone reduction of between 3 and 10% in agreement with previous studies. EPP is found to modulate the radiative solar cycle effect in the middle atmosphere in a significant way, bringing temperature and ozone variations closer to observed patterns. The Southern Hemisphere polar vortex undergoes an intensification from solar minimum to solar maximum instead of a weakening. This changes the solar cycle variation of the Brewer-Dobson circulation, with a weakening during solar maxima compared to solar minima. In response, the tropical tropopause temperature manifests a statistically significant solar cycle variation resulting in about 4% more water vapour transported into the lower tropical stratosphere during solar maxima compared to solar minima. This has implications for surface temperature variation due to the associated change in radiative forcing.

1 Introduction

Although the field of research on the influence of solar radiation and particle flux on the atmosphere is fast growing, great uncertainty remains concerning impacts and the mechanisms involved. Traditionally, modeling studies of solar variability effects on the climate system have focused on two basic ideas: (1) direct forcing of the troposphere by surface warming associated with changes in the total solar irradiance (TSI) or, in a more complex scenario, modulation of the atmosphere-ocean interactions producing internal oscillations (see for example White et al., 1997; White, 2006); and (2) forcing of the stratosphere associated with changes in ultraviolet (UV) radiation causing

ACPD

10, 24853–24917, 2010

EPP impact on the middle atmosphere

K. Semeniuk et al.

Title Page

Abstract

Introduction

Conclusions

References

Tables

Figures

◀

▶

◀

▶

Back

Close

Full Screen / Esc

Printer-friendly Version

Interactive Discussion



EPP impact on the middle atmosphere

K. Semeniuk et al.

[Title Page](#)[Abstract](#)[Introduction](#)[Conclusions](#)[References](#)[Tables](#)[Figures](#)[◀](#)[▶](#)[◀](#)[▶](#)[Back](#)[Close](#)[Full Screen / Esc](#)[Printer-friendly Version](#)[Interactive Discussion](#)

an increase in ozone and associated warming during solar maximum conditions. The latter results in changes in the latitudinal distribution of UV heating in the stratosphere which modifies the Eliassen-Palm flux divergence leading to a reduction of the Brewer-Dobson circulation (Kodera and Kuroda, 2002; Kuroda and Kodera, 2002; Kodera and Shibata, 2006). Both (1) and (2) operate at the same time increasing the complexity of the system response. An extensive model based analysis exploring the different effects and its implications is provided by Rind et al. (2008), which clearly demonstrates our current lack of understanding of the details of how each mechanism operates individually and the impacts of coupled processes. Indeed, Kodera et al. (2008) find that CO₂ mediated cooling of the stratosphere produces a tropospheric response through a nonlinear interaction with the solar cycle.

Recently, more attention has been devoted to the effects of upper atmosphere NO_x and HO_x produced from ionization by energetic particle precipitation (EPP) on stratospheric ozone. As with UV irradiance, the EPP component of the solar cycle has the potential to influence the tropospheric response through dynamical processes in the stratosphere that are sensitive to the ozone distribution (Callis et al., 2001; Shindell et al., 1999).

Ionization by energetic particle precipitation in the atmosphere is an ubiquitous feature of the Sun-Earth system. The work by Warneck (1972), Swider and Keneshea (1973) and Crutzen et al. (1975) pioneered research into influence of energetic particle precipitation on the chemistry of the atmosphere through the enhancement of NO_x. Following this early work, Solomon and Crutzen (1981) and Solomon et al. (1981, 1983) pointed out a coupling mechanism whereby thermospheric NO_x could affect the stratosphere. The Halogen Occultation Experiment (HALOE) instrument on the Upper Atmosphere Research Satellite (UARS), and the subsequent Atmospheric Trace Molecule Spectroscopy (ATMOS) and Polar Ozone and Aerosol Measurement (POAM) experiments provided observational evidence for EPP associated NO_x enhancement (Callis et al., 1996; Randall et al., 1998, 2001; Rinsland et al., 1996; Russell et al., 1984). However, due to the complex nature of the problem, little effort was devoted to

EPP impact on the middle atmosphere

K. Semeniuk et al.

Title Page

Abstract

Introduction

Conclusions

References

Tables

Figures

◀

▶

◀

▶

Back

Close

Full Screen / Esc

Printer-friendly Version

Interactive Discussion



the inclusion of EPP effects in chemistry climate models. This has changed in recent years prompted by conclusive observational evidence of significant NO_x enhancement in the polar regions, extending to stratospheric altitudes, during major solar proton events (e.g., Siskind, 2000; Randall et al., 2001, 2005; Hauchecorne et al., 2005, 2007; Jackman et al., 2005; López-Puertas et al., 2005). A number of 1, 2 and 3-dimensional model studies, mostly focused on a particular event and sometimes using measured NO_x enhancement to force the model have been conducted since then (for a literature review see Jackman et al., 2008; Reddmann et al., 2010).

The main difficulty in implementing energetic particle precipitation forcing in general circulation models is the complexity of the D region ion chemistry. One feasible option is to use parameterizations, relating ionization rates to the production of NO_x and HO_x (e.g., Jackman et al., 2008). The inclusion of ionization by energetic particles in global self-consistent chemistry climate models started with the work of Rozanov et al. (2005), and has been done differently in different models. For example, while the WACCM implementation described by Marsh et al. (2007) includes thermospheric NO_x chemistry explicitly, it does not account for stratospheric production of NO_x and HO_x due to penetration of high energy galactic cosmic ray particles. The implementation in the HAMMONIA model, as described in Schmidt et al. (2006), includes stratospheric NO production by galactic cosmic rays following Heaps (1978) and has the thermospheric NO production based on the scheme of Huang et al. (1998), with the parameters adjusted to reproduce the Student Nitric Oxide Explorer (SNOE) satellite instrument measurements (Barth et al., 2003).

HO_x is relatively short-lived (of the order of days) leading mostly to local effects, while NO_x can lead to both short and long term (order of months) catalytic ozone destruction in the middle atmosphere. A comprehensive study of the short, middle and long term effects of large solar proton events (SPEs) in the polar regions has been conducted by Jackman et al. (2008, 2009) involving model and measurements. Ozone destruction in the stratosphere can exceed 10% and last up to 5 months depending of the magnitude of the event. Based on their work it is apparent that CCMs are not able to reproduce all

the features found by satellite measurements of atmospheric composition. Indeed, the work of Callis et al. (2001) demonstrates that SPEs are not the only type of EPP that can have a significant impact on ozone in the stratosphere and that auroral electron precipitation also needs to be taken into account.

5 The multi-model study of solar variability effects by Austin et al. (2008) indicates that chemistry climate models forced with monthly observed sea surface temperatures and monthly or daily variations in solar irradiance are able to capture the tropical stratosphere ozone response reasonably well. While it appears that EPP effects are not of primary importance to the ozone response in the tropics, this says little about the importance of EPP for the evolution of polar vortices and Brewer-Dobson circulation.

10 As noted above, there is a growing body of work into the effects of EPP on the middle atmosphere. However, to the best of our knowledge there is no published analysis focused on the global role of EPP, including galactic cosmic rays, coupled with the solar cycle evolution of the atmosphere in a chemistry climate model. The modulation of the solar irradiance cycle impact on the atmosphere by EPP is the focus of the work presented here.

15 We conduct pseudo-timeslice ensemble simulations, which include the solar cycle irradiance variation alone and those that also include EPP, using the Canadian Middle Atmosphere Model (CMAM). CMAM is a chemistry climate model which has been modified to include the solar irradiance cycle in the solar heating and photolysis rates as described below. Three types of EPP were included in the model: auroral electrons, solar proton events (SPEs) and galactic cosmic rays (GCR). The EPP effect on the model chemistry is related to the amount of energy deposition, and hence ionization, which can be converted into production of atomic nitrogen (Porter et al., 1976) and HO_x (Solomon and Crutzen, 1981). For aurora and SPEs, the vertical profile of the energy deposition is inferred from electron and proton fluxes, observed in low earth orbit and in geostationary orbit, respectively. For GCR we use the Usoskin and Kovaltsov (2006) parameterization for ionization, which is also based on observations. More details of the model and EPP parameterizations are given in the next section.

EPP impact on the middle atmosphere

K. Semeniuk et al.

Title Page

Abstract

Introduction

Conclusions

References

Tables

Figures



Back

Close

Full Screen / Esc

Printer-friendly Version

Interactive Discussion



2 Description of the model and simulations

The CMAM version used here has a spectral dynamical core with a triangular truncation of 31 spherical harmonics. There are 71 sigma-pressure hybrid levels extending from the surface to about 95 km. A non-zonal sponge layer is applied in the upper two pressure scale heights of the model. The radiation scheme of the model takes into account processes which are essential in both the troposphere and middle atmosphere. A more detailed description of the CMAM dynamical core and radiation scheme is given by Beagley et al. (1997) and Fomichev et al. (2004), respectively.

The CMAM has a comprehensive middle atmosphere photochemical scheme (de Grandpré et al., 1997, 2000) which can capture NO_x and HO_x production and decay, as well as interaction with chlorine and bromine chemistry (Melo et al., 2008; Brohede et al., 2008). However, tropospheric chemistry is limited to gas phase reactions. Removal of species is by dry deposition at the surface. There is no chemistry with volatile organic compounds and other aerosols. Surface and lightning emissions of NO_x are absent. Nevertheless, we note that the tropospheric ozone field generated is reasonable (de Grandpré et al., 2000).

The model has a reasonable mesospheric and stratospheric climate; specifically major sudden stratospheric warmings (SSWs) are captured with a realistic incidence rate (McLandress and Shepherd, 2009). SSWs are important for NO_x transport from the upper mesosphere to the stratosphere due to the associated intensification of polar vortex in the mesosphere resulting in more effective polar night confinement (Hauchecorne et al., 2007; Semeniuk et al., 2008; Randall et al., 2009). Analysis of the impact of EPP on the frequency of occurrence of SSWs will be presented in a subsequent paper.

For the simulations conducted for this study sea surface temperatures, sea ice and chemical boundary conditions were specified to be repeated 1979 values from the WMO A1B greenhouse and AB halogen scenarios (Eyring et al., 2007). To investigate the impact of individual EPP types single realization runs without solar cycle irradiance variation were conducted over the 1979 through 2006 period for aurora, SPEs, GCR

EPP impact on the middle atmosphere

K. Semeniuk et al.

Title Page

Abstract

Introduction

Conclusions

References

Tables

Figures

◀

▶

◀

▶

Back

Close

Full Screen / Esc

Printer-friendly Version

Interactive Discussion



and a reference case without EPP. The results are presented in Sect. 4.

The role of EPP in the 11-year solar cycle impact on the atmosphere was analyzed further with ensemble simulations. A three member ensemble simulation from 1979 through 2006 without EPP but with solar cycle irradiance variation is taken as the reference. A three member ensemble simulation over the same period but with all three types of EPP included together is taken as the perturbation. Effects on the long term mean state as well as variation with the solar cycle are presented in Sect. 5.

2.1 Solar irradiance scheme

The incident solar radiation at the top of the atmosphere varies on different time scales. Variations in the total solar irradiance (TSI), i.e. the spectrally integrated solar irradiance, over the 11-year solar cycle are very small (with an amplitude of approximately 0.1%). However, as noted above, variations in solar irradiance are spectrally dependent and increase considerably with decreasing wavelength in the ultraviolet (UV) part of the spectrum, reaching several percent in ozone absorption bands between 200 and 300 nm and exceeding 10% in the molecular oxygen bands at wavelengths shorter than 200 nm (e.g., Fröhlich and Lean, 2004). To take into account the spectral variability of the solar radiation, both the solar heating and photolysis rates schemes have been modified.

Absorption of solar UV radiation at wavelengths shorter than 300 nm by ozone and molecular oxygen provides the main contribution to the solar heating of the middle atmosphere (e.g., Fomichev, 2009). This means that in order to simulate effects of solar variability in the middle atmosphere, the spectral resolution of the model radiation scheme should be high enough so that it allows for an adequate description of variations in the spectral solar irradiance (SSI) over the solar cycle evolution (e.g., Egorova et al., 2004; Nissen et al., 2007). However, the shortwave radiation scheme of the CMAM exploits only one spectral band between 250 and 690 nm and uses TSI as the solar input for solar heating calculations. This approximation reflects the historical focus of numerical global modeling on the troposphere where absorption of solar UV

EPP impact on the middle atmosphere

K. Semeniuk et al.

Title Page

Abstract

Introduction

Conclusions

References

Tables

Figures

◀

▶

◀

▶

Back

Close

Full Screen / Esc

Printer-friendly Version

Interactive Discussion



radiation was thought to play only a very minor role, given the much lower intensity in the UV spectral region compared to the visible and near-infrared parts of the solar spectrum.

In order to properly account for solar input in the current study, a scheme allowing for calculation of variability in solar heating due to variations in SSI at wavelengths shorter than 300 nm has been developed. This scheme takes into account absorption of direct radiation in eight spectral bands between 121 and 300.5 nm (121–122, 125–152, 152–166, 166–175, 175–206, 206–242.5, 242.5–277.5, and 277.5–305.5 nm) and agrees very well with the reference line-by-line calculations (Fomichev et al., 2010).

Figure 1 presents time series of the solar heating rate deviation from the 1950–2006 mean values at different heights as calculated with the developed scheme. Calculations were done for an equatorial ozone profile and an overhead Sun assuming 24 h illumination with the use of daily varying SSI provided on the SOLARIS website (2008). Changes in solar heating associated with changes in TSI (blue) and in SSI (green) are shown. As seen from Fig. 1, taking into account variability in TSI only provides a reasonable solar heating signal in the troposphere, where absorption in visible and near-infrared regions dominates the heating rates, but significantly underestimates it in the middle atmosphere. In this case the signal is very small (less than 0.0012 K/day from solar minimum to maximum at 8 km) and has a relatively weak variation with height. With variability in SSI included, the solar signal considerably increases with height as absorption at shorter wavelengths becomes more important. In this case, the short-wave heating rates between solar minimum and maximum vary by about 0.03, 0.3 and 1 K/day at 32, 48 and 80 km levels, respectively.

To calculate photolysis rates, the CMAM chemistry scheme uses a look-up table in which photo-dissociation rates are provided for 165 spectral intervals with a width ranging from 1 to 10 nm between 121 and 852.5 nm. These spectral ranges and spectral resolution are quite sufficient for the purpose of solar variability studies. For the current study, the photolysis scheme has been modified to calculate the look-up table daily reflecting changes in the SSI. Thus, a reasonable solar forcing is provided in the

EPP impact on the middle atmosphere

K. Semeniuk et al.

Title Page

Abstract

Introduction

Conclusions

References

Tables

Figures

◀

▶

◀

▶

Back

Close

Full Screen / Esc

Printer-friendly Version

Interactive Discussion



model.

2.2 EPP parameterization

In these simulations we limit our ionization sources to auroral electrons, solar coronal mass ejection protons and galactic cosmic rays. Electron fluxes are measured by NOAA low earth orbit satellites, proton fluxes are measured by the NOAA GOES geostationary satellites, and galactic cosmic ray intensity is measured by surface neutron monitors.

For all EPP types the NO_x and HO_x production rates were determined from the energy deposition rate, E ($\text{eVg}^{-1}\text{s}^{-1}$), following the work of Porter et al. (1976). The ionization rate, I ($\text{cm}^{-3}\text{s}^{-1}$), is given by

$$I = \frac{\rho E}{35.4} \quad (1)$$

where ρ is the air density in g cm^{-3} and the ionization energy is 35.4 eV. The production of NO_x is given by

$$P_{\text{NO}_x} = 1.25I \quad (2)$$

and 45% of P_{NO_x} is assumed to produce $\text{N}(^4\text{S})$ while 55% is assumed to go into $\text{N}(^2\text{D})$. The latter is added to the production of NO and O since the reaction of $\text{N}(^2\text{D})$ with O_2 to form these products is rapid compared to the reaction of $\text{N}(^4\text{S})$ with O_2 , which is very temperature dependent. The production of HO_x is given by

$$P_{\text{HO}_x} = aI \quad (3)$$

where $a(z)$ is a height dependent function that varies from a value of 2 at 40 km to zero above 90 km and is taken from Solomon and Crutzen (1981). It is assumed that P_{HO_x} contributes equally to the production of H and OH . Below 40 km, $a(z)$ is taken to have a constant value of two. This assumption is a limitation since work with detailed ion

EPP impact on the middle atmosphere

K. Semeniuk et al.

Title Page

Abstract

Introduction

Conclusions

References

Tables

Figures

◀

▶

◀

▶

Back

Close

Full Screen / Esc

Printer-friendly Version

Interactive Discussion



chemistry models (Stiller et al., 2005; Verronen et al., 2006) indicates that HNO_3 is an important direct product through ion cluster and/or ion-ion recombination reactions with secondary OH production via photodissociation. As noted by Verronen et al. (2006) assuming a constant HO_x production leads to an underestimation of HO_x production during sunrise and sunset which also affects ozone loss, but only lasts for a short period outside polar regions.

Figure 2 shows the time series of the ion pair production rate for the three types of EPP used in the model along with the F10.7 solar variability index. Auroral activity maximizes during the descending stage of the solar cycle. SPEs tend to cluster during solar maximum years when coronal activity is enhanced. GCR is anti-correlated with the solar cycle due to the complex heliospheric modulation driven by solar magnetic activity.

The vertical profiles of the peak ion pair production rate are shown in Fig. 3 based on the parameterizations described below. Auroral ionization maximizes in the upper mesosphere and above with a high energy tail that penetrates into the lower mesosphere. SPEs can have maximum ionization near the stratopause depending on the energy spectrum of the solar protons (Jackman et al., 2005). The GCR profiles peak around 13 km and there is about a factor of two difference between solar maximum and minimum conditions.

2.2.1 Aurora

For aurora the daily energy deposition is inferred from daily composites of electron flux observations from the Medium Energy Proton and Electron Detector (MEPED) instruments on NOAA low earth orbit satellites in the 30–100 keV, 100–300 keV and 300–1000+ keV channels (Seale and Bushnell, 1987). The MEPED data from 1979 through 2006 was used (NOAA/POES website, 2008). Data gaps were filled using the method of singular spectrum analysis (Kondrashov and Ghil, 2006).

The lowest energy channel was not used as electrons with this energy are deposited primarily above 100 km and the model lid. The contribution of the region above the

EPP impact on the middle atmosphere

K. Semeniuk et al.

Title Page

Abstract

Introduction

Conclusions

References

Tables

Figures

◀

▶

◀

▶

Back

Close

Full Screen / Esc

Printer-friendly Version

Interactive Discussion



EPP impact on the middle atmosphere

K. Semeniuk et al.

Title Page

Abstract

Introduction

Conclusions

References

Tables

Figures

◀

▶

◀

▶

Back

Close

Full Screen / Esc

Printer-friendly Version

Interactive Discussion



model lid to lower altitudes is reduced for two reasons. Firstly, during descent in the lower thermosphere and upper mesosphere region air parcels experience large meridional excursions through tidal and gravity wave action. This leads to significant loss of NO_x through mixing into lower latitudes and photochemical conversion back into N_2 . The shadowing effect of the Earth on the atmosphere changes with height so that for higher solar zenith angles while the stratosphere is in darkness the lower thermosphere is still illuminated. Thus, the area that can be considered to be in polar night is reduced. Secondly, the density decreases exponentially with height. In the vicinity of the mesopause, between 80 and 90 km, the scale height is about 4 km, so the atmospheric density experiences about a 30-fold reduction between 80 and 100 km. Any conservative tracer originating above 100 km will experience a similar or greater reduction factor in mixing ratio during descent to 80 km depending on horizontal mixing.

A vertical energy deposition profile was derived using peak flux values from twelve 30° longitudinal sectors at each altitude. The average of these twelve peak electron flux values was used for subsequent calculations. The dependence of the flux on energy was approximated by a piece-wise exponential fit following Callis et al. (1998). The energy deposition was obtained using the range-energy expression from Gledhill (1973) and using the 80° -isotropic energy distribution function from Rees (1989).

A parametrized auroral oval was used to obtain a 3-D distribution of electron energy deposition from the vertical profile calculated. The auroral oval is a modified version of the scheme from Holzworth and Meng (1975) based on the formulation of Feldstein (1963). The modification for the auroral horizontal distribution, H , was as follows:

$$H(\phi, \theta) = \begin{cases} \exp(-((\theta_g(\phi, \theta) - \theta_c)/\delta\theta_p)^2), & \text{if } \theta_g > \theta_c \\ \exp(-((\theta_g(\phi, \theta) - \theta_c)/\delta\theta_e)^2), & \text{if } \theta_g \leq \theta_c \end{cases} \quad (4)$$

$$\begin{aligned} \theta_c &= \theta_e + 0.3(\theta_p - \theta_e) \\ \delta\theta_p &= 2(\theta_p - \theta_c) \\ \delta\theta_e &= (\theta_c - \theta_e) \end{aligned} \quad (5)$$

EPP impact on the middle atmosphere

K. Semeniuk et al.

Title Page

Abstract

Introduction

Conclusions

References

Tables

Figures

◀

▶

◀

▶

Back

Close

Full Screen / Esc

Printer-friendly Version

Interactive Discussion



where θ_e and θ_p are the equatorial and polar corrected geomagnetic latitude limits of the auroral oval, respectively, from the Holzworth and Meng (1975) scheme. This modification was made to improve the realism of the auroral oval distribution. The map from geographic longitude (ϕ) and latitude (θ) on the model grid to corrected geomagnetic latitude ($\theta_g(\phi, \theta)$) was calculated offline using an updated version of the GEOCGM program of Tsyganenko et al. (1987).

Hourly values of the auroral electrojet (AE) index (WDC website, 2008) were used to specify the size of the oval using the relation for the Q index from Starkov (1981). The orientation of the oval follows the Sun. The parameterized auroral oval resets Q values to six when they exceed this number, so that more NO_x is deposited in the polar night than should be during intense geomagnetic storms. In addition, the highest energy electrons are assumed to be distributed in the same auroral oval as the lower energy electrons when in fact relativistic electrons are deposited in the sub-auroral belt (e.g., Brown, 1966). However, the relativistic electrons account for a small fraction of the NO_x production and this limitation of the scheme is not significant.

2.2.2 SPEs

For SPEs the daily energy deposition rate vertical profiles were obtained from the dataset of Jackman (2006). The horizontal distribution of the energy deposition was approximated by axially symmetric caps centered on the geomagnetic poles with a diameter of about 60 degrees (Jackman et al., 2005). A smooth Gaussian squared transition was assumed between 25° and 45° away from the geomagnetic poles with a 5° scaling factor to minimize Gibbs fringing (CMAM uses spectral transport).

2.2.3 GCR

Ionization effect of GCR was computed using the CRAC:CRII (Cosmic Ray induced Atmospheric Cascade: Application for Cosmic Ray Induced Ionization) model (Usoskin and Kovaltsov, 2006) extended toward the upper atmosphere (Usoskin et al., 2010).

EPP impact on the middle atmosphere

K. Semeniuk et al.

Title Page

Abstract

Introduction

Conclusions

References

Tables

Figures

◀

▶

◀

▶

Back

Close

Full Screen / Esc

Printer-friendly Version

Interactive Discussion



The model is based on the full Monte-Carlo simulation of the cosmic ray induced atmospheric cascade and provides computations of the ionization rate in 3-D. The accuracy of the model is within 10% in the troposphere and lower stratosphere, and up to a factor of two in the upper atmosphere – mesosphere (Bazilevskaya et al., 2008). The temporal variability of the GCR energy spectrum, which is a result of the solar modulation in the heliosphere, is parameterized via the variable modulation potential, which is computed on a monthly basis using the data from the world network of ground-based neutron monitors (Usoskin et al., 2005). The final time-dependent ionization rate was computed using the following parameters: altitude (quantified via the barometric pressure), geomagnetic latitude (quantified via the geomagnetic cutoff rigidity computed in the framework of IGRF-10 model (IAGA/V-MOD website, 2008) and solar activity (quantified via the modulation potential).

3 Regression model

Following the analysis in Austin et al. (2008), we use a linear multiple regression model with first order autoregressive, AR(1), error treatment (Tiao et al., 1990) to investigate the solar cycle in key model fields. However, instead of subtracting the mean seasonal variation we include annual and semiannual harmonics. As CMAM simulations do not resolve the QBO and do not contain long term variation of aerosols and sea surface temperatures no fitting is done for QBO, aerosol surface area and El Niño/Southern Oscillation (ENSO). But QBO, aerosol and ENSO terms are used when fitting the observational data. Thus, for a timeseries of a field, e.g. ozone, M , we have

$$\begin{aligned}
 M = & a_0 + a_1 \sin(\pi \frac{t}{2}) + a_2 \cos(\pi \frac{t}{2}) + a_3 \sin(\pi t) + \\
 & a_4 \cos(\pi t) + bt + cS_{F10.7} + \\
 & d_1 U_{QBO1} + d_2 U_{QBO2} + eSAD + fMEI + e
 \end{aligned} \quad (6)$$

where t is in seasons (three month means), $S_{F10.7}$ is the F10.7 coronal index normalized by 100, and U_{QBO1} and U_{QBO2} are based on the 30 hPa Singapore winds as 24865

in Randel and Wu (2007). The remaining fitting terms are the sulphate surface area density at 60 hPa, SAD, (Hamill et al., 2006) and the Multivariate ENSO index, MEI, (Wolter and Timlin, 1998).

The height-latitude distributions of the F10.7 regression coefficient, c , are shown in Sect. 5. This coefficient represents the fraction of the timeseries variation that projects onto the F10.7 timeseries. We chose the F10.7 index as a general representation of the solar cycle. The A_p index may give a better fit for the auroral component, as it reflects the variation of the solar wind streams, but is not advantageous for SPEs and GCR.

4 Impact of individual EPP types

The effect of the three EPP types on the long-term composition and dynamics is presented in this section. These runs are single realizations from the 1979 through 2006 period spanned by the EPP data. This 28 year period is too short to have a high confidence level for the dynamical response given dynamical variability. However, they do reveal the distribution of the impact on composition and give some idea of the dynamical sensitivity.

4.1 Aurora

The run mean, July through August mean (JJA) zonal wind, temperature and the transformed Eulerian mean (TEM) mass streamfunction, which represents the Brewer-Dobson circulation (Andrews et al., 1987), for the run with auroral ionization and the reference run (no ionization, no solar cycle) are shown in Fig. 4 (left panels). There is a small but statistically significant reduction in the strength of the SH polar vortex (Fig. 4, top left panel) as measured by the reduction in the zonal wind and also by the increase in temperature below 60 km (Fig. 4, middle left panel). The mass streamfunction shows a statistically significant increase poleward of 50° S below 30 km, which is consistent

EPP impact on the middle atmosphere

K. Semeniuk et al.

Title Page

Abstract

Introduction

Conclusions

References

Tables

Figures

◀

▶

◀

▶

Back

Close

Full Screen / Esc

Printer-friendly Version

Interactive Discussion



EPP impact on the middle atmosphere

K. Semeniuk et al.

Title Page

Abstract

Introduction

Conclusions

References

Tables

Figures

◀

▶

◀

▶

Back

Close

Full Screen / Esc

Printer-friendly Version

Interactive Discussion



with the increased temperature and weaker zonal wind above 20 km and suggests an increase in wave drag, or more negative Eliassen-Palm flux divergence, is responsible for the dynamical changes rather than direct radiative effects from chemical constituent changes. Note that in the SH negative anomalies in the mass streamfunction indicate intensification in contrast to the NH where this applies to positive anomalies due to the change in sign of the Coriolis parameter at the equator. It is also notable that the Brewer-Dobson circulation change in the SH appears to be hemispheric in scale in spite of the fact that the ionization impact on composition occurs at high latitudes (see Figs. 5 and 6).

In contrast to JJA, for the December through February (DJF) period there is no significant response in the NH polar vortex, temperature and Brewer-Dobson circulation (not shown). The NH polar vortex tends to be weaker and more disturbed compared to the SH vortex due to hemispheric differences in planetary wave forcing (Andrews et al., 1987). So perturbations associated with composition changes, unless they are large, are not likely to alter the NH state significantly. As noted above, the more disturbed NH vortex results in increased destruction of auroral NO_x by exposure to sunlight during descent as air parcels are transported out of the polar night by planetary wave induced mixing and vortex deformation. So the chemical impact on dynamics is more limited in the NH compared to the SH as will be shown below.

The DJF mean, run mean NO_y , HO_x and ozone differences for the run with auroral ionization and the reference run are shown in Fig. 5 (left panels). There is a large increase of NO_y in the winter auroral production zone down to about 30 km. We note that above 40 km the NO_y is essentially NO_x . In the summer auroral production zone the increase extends only down to 65 km. The difference in the polar regions between the summer and winter is, of course, that the exposure of NO_x to sunlight in the polar summer results in its cannibalistic destruction, viz.,



which is modulated by reaction with O₂ and OH,



There is also a significant increase of NO_x at all latitudes above 70 km. In the summer hemisphere at middle and polar latitudes and between the surface and 20 km, NO_y increases by over 5% and this feature is a remnant of downward transport of NO_y during the previous winter. In the Northern Hemisphere during winter, below 40 km, there is a modest decrease of NO_y in this latitude range (but not statistically significant) which may be associated with a strengthening of the Brewer-Dobson circulation (not shown but also not statistically significant). Since the disturbed state of the winter NH stratosphere prevents significant transport of NO_y into this region from above, an increase in transport of low NO_y air from the tropics could lead to this reduction.

The left central panel for HO_x shows an increase in both the summer and winter polar mesosphere due to the EPP HO_x source from water vapour. The largest percentage increase occurs in the winter polar regions partly due to the reduced background HO_x in winter. Above 70 km at low and middle latitudes there is no comparable increase of HO_x as compared to NO_x. The HO_x source in this region is dominated by photolysis of water vapour. Also, to a lesser extent, the difference is because the photochemical lifetime of HO_x is shorter (under a day in contrast to 5 days for NO_x).

In the summer hemisphere, below 40 km there is a decrease in HO_x. This may be due to changes in the sources and/or sinks of HO_x. As can be seen in the lowest left panel, ozone has also decreased and so one of the sources of HO_x, viz. reaction of O(¹D) (produced from photolysis of ozone) with H₂O, CH₄ and H₂ would decrease. There is also a source from the photolysis of HNO₃, which has increased in this region (top left panel, NO_y is primarily HNO₃ at these altitudes). With respect to changes in sinks, the sink via the reaction OH + HNO₃ → H₂O + NO₃ has increased as well.

The lowest left panel shows that the largest effect on ozone is in the winter polar region above 50 km. This reflects that auroral electron ionization occurs in the upper

EPP impact on the middle atmosphere

K. Semeniuk et al.

Title Page

Abstract

Introduction

Conclusions

References

Tables

Figures

◀

▶

◀

▶

Back

Close

Full Screen / Esc

Printer-friendly Version

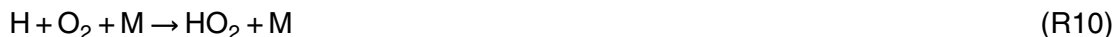
Interactive Discussion



mesosphere polar regions and the HO_x produced (see middle left panel) leads to the direct and indirect reduction of ozone via



and



This effect can also be seen in the summer polar region above 60 km. There is ozone loss of between 2 and 5% between 25 and 40 km in both the winter and summer hemispheres. The additional ozone loss is driven by increases in NO_x that survived from the previous winter via



There is a transition from O₃ destruction to production in the lowermost stratosphere and troposphere (Basseur and Solomon, 2005). Above roughly 20 km the NO_x loss cycle (R12–R14) dominates while below the O₃ smog production reactions become important, e.g.



24869

EPP impact on the middle atmosphere

K. Semeniuk et al.

Title Page

Abstract

Introduction

Conclusions

References

Tables

Figures

◀

▶

◀

▶

Back

Close

Full Screen / Esc

Printer-friendly Version

Interactive Discussion



Thus, the increase in NO_x below 20 km leads to an increase of ozone. The decrease in the HO_x is more than compensated by the increase in NO_x .

Figure 6 shows the atmospheric response for the run mean of the opposite season, JJA. In general, the pattern is not just a simple mirror reflection about the equator as might be anticipated. For example, the penetration of extra NO_x in the SH polar winter is more contained within the vortex than for DJF in the NH. In addition, the increase and penetration in the SH winter extends to 30 km for a 80% change compared to 45 km in the NH winter. The SH summer NO_x is higher than for NH summer. This is consistent with the higher levels transported during winter in the SH surviving through the following summer.

As expected, there is an increase in HO_x in the SH winter polar region as a result of EPP and the small background HO_x in the reference run. There is also a small enhancement in the NH summer polar region. In the NH winter, there is a 5% decrease in HO_x in mid-latitudes between 50 and 70 km. Another region of decrease occurs between 30 and 40 km. For the SH winter, the decrease has strengthened and also has become more extensive in the stratosphere extending below 20 km. Above 60 km, HO_x is produced by photolysis of H_2O . Below 60 km it is largely through reaction of $\text{O}(^1\text{D})$ with H_2O , CH_4 and H_2 . This would suggest that $\text{O}(^1\text{D})$ has decreased and to some extent this is reflected by the reduction of ozone in polar regions in SH winter. Whereas there is a substantial decrease in HO_x in the SH winter between 10 and 40 km, there is a much smaller decrease of HO_x in the NH winter polar regions.

The SH ozone decrease in the polar vortex (Figs. 5 and 6, left panels) is caused in the upper regions by HO_x increases while in the lower regions it is due to increased NO_x since HO_x does not survive transport from the mesosphere into the stratosphere. Below 20 km at all latitudes in JJA there appears to be an enhancement of ozone but of low statistical significance. However, it is compatible with the increase of NO_x and also could be due to the smog reactions noted above in addition to increased transport of O_3 by the enhanced Brewer-Dobson circulation (Fig. 4, bottom left panel). The stronger circulation also leads to more ozone transport to the troposphere from the stratosphere

EPP impact on the middle atmosphere

K. Semeniuk et al.

Title Page

Abstract

Introduction

Conclusions

References

Tables

Figures

◀

▶

◀

▶

Back

Close

Full Screen / Esc

Printer-friendly Version

Interactive Discussion



which would contribute to the chemical ozone increase.

4.2 SPEs

From the difference plots in Fig. 4 (middle panels) it can be seen that for the SPEs case the SH winter polar vortex is weakened in high latitudes and also becomes broader judging by the larger increase in the zonal wind equatorward of 60° S. The peak negative zonal wind anomaly is comparable to the auroral case. However, the temperature change is weaker and not statistically significant near the pole but is statistically significant in middle latitudes between 20 and 40 km. There is also a warming in the tropics not present in the auroral case in this layer. This middle latitude cooling and tropical warming appears to be due to the weakening of the residual circulation in middle and low latitudes in this layer of the stratosphere (Fig. 4, lower panel). The Brewer-Dobson circulation shows an intensification similar to the auroral case in high latitudes below 40 km with some statistical significance below 30 km.

Figure 5 (middle panels) shows the differences in NO_y , HO_x and ozone for SPEs in DJF. The SPEs NO_x response pattern is similar to, but much weaker, than that of the auroral case for the mesosphere. Even though there is more ionization produced by individual SPEs in the upper stratosphere and lower mesosphere during each event, it is sporadic and averages out to similar or lower values over the duration of the simulation. In addition, the SPEs NO_x is formed lower in the atmosphere and so a given amount created will appear with a lower mixing ratio near the stratopause as compared to the mesopause. The low values of NO_x above 70 km in the NH are due to both downward transport from the lower thermosphere where the model lid boundary condition is 1 ppmv, and the fact that SPEs ionization peaks around 60 km so there is much less ionization above 70 km compared to aurora. The higher values of NO_x above 70 km in the summer hemisphere (here the NH) are due to the meridional circulation pattern. There is upwelling in the summer polar regions, which lofts the NO_x in the mesosphere with transport above the mesopause.

EPP impact on the middle atmosphere

K. Semeniuk et al.

Title Page

Abstract

Introduction

Conclusions

References

Tables

Figures

◀

▶

◀

▶

Back

Close

Full Screen / Esc

Printer-friendly Version

Interactive Discussion



EPP impact on the middle atmosphere

K. Semeniuk et al.

[Title Page](#)[Abstract](#)[Introduction](#)[Conclusions](#)[References](#)[Tables](#)[Figures](#)[◀](#)[▶](#)[◀](#)[▶](#)[Back](#)[Close](#)[Full Screen / Esc](#)[Printer-friendly Version](#)[Interactive Discussion](#)

A NO_y increase between 2 and 7% is present in the SH from the surface to 40 km. There is some accumulation above the extratropical tropopause as with the case of aurora. Between 15 and 25 km in the SH polar region the response is negative but with no statistical confidence. This suggests a high level of variability in this region for this season which is likely due to dynamical processes.

The SPEs HO_x response shows an increase in the polar lower mesosphere and upper stratosphere since it is being produced in this region in contrast to the case with aurora. Below 40 km there is a decrease in HO_x through reaction of OH with HNO_3 , which has been augmented. There is also a reduction in ozone, the source of $\text{O}(^1\text{D})$ (and thus HO_x), in this region. There is a large correlation between the distribution of the NO_y and HO_x anomalies.

The ozone response is concentrated in the polar regions as for the auroral case. As expected from the intermittency of SPEs the response is weaker but the difference is not large. There is a roughly 3% decrease near the winter pole around 30 km. As with the auroral case, there is a similar reduction near the summer pole at this height. However, SPEs occur both summer and winter producing in situ effects not dependent on transport from the upper mesosphere, so this feature is not simply a memory from the previous winter. In the troposphere, there is an increase of ozone which could be due to increased NO_x but the effects of an increased Brewer-Dobson circulation could also be important. However, the changes are not statistically significant.

For JJA NO_y and HO_x changes (Fig. 6) the response is almost the mirror of DJF changes (Fig. 5). For JJA, the ozone impact is not as pronounced as for the case of aurora and is only statistically significant between 20 and 30 km (cf. lower middle and lower left panels of Fig. 6). This reflects the fact that the SPEs are sporadic. It also suggests that the containment properties of the stronger SH polar vortex for NO_x produced by SPEs are less important since the NO_x production (in the lower mesosphere and upper stratosphere) occurs in a region shielded from UV destruction. The JJA vortex response (Fig. 4, top middle panel) suggests that ozone perturbations of a few percent in the polar region between 20 and 30 km can both induce a weakening

of the strength and an increase of the diameter of the SH polar vortex above 25 km.

Vortex variability does play a role in the SPEs case as can be seen by the absence of a significant ozone loss in the NH summer: any NO_x produced during the previous winter at higher altitudes experiences greater loss compared to the SH. Between the tropopause and 25 km during DJF in the SH there is an ozone increase of 3 to 10% which is statistically significant at the 80% confidence level (contours not shown). At these heights this increase is likely due to the smog reactions on account of the NO_x increase (about 5%), which more than balances the HO_x decrease. This summertime ozone increase is smaller in scale in the NH.

4.3 GCR

The dynamical response in JJA shows some similarities to the other two EPP types (Fig. 4, right panels). The polar vortex weakens to a similar degree between 60°S and 80°S above 30 km. But the reduction is not associated with a vortex diameter increase and there is a weakening in middle and low latitudes as well. The temperature change in the SH reaches lower latitudes and it appears that the wave drag change is broader meridionally compared to the auroral and SPEs cases. The GCR temperature change is most similar to that produced by aurora, but with a large region of statistically significant cooling in the tropics and subtropics of the stratosphere. The residual circulation intensification in the SH extends over the depth of the stratosphere with a 95% confidence region between the tropopause and 40 km poleward of 60°S . GCR is producing a change of the same sign in wave drag over a broader latitude span in spite of being a weaker source of ionization than the other two types of EPP. As shown below, the GCR effect on ozone is not confined to the polar regions.

The DJF and JJA chemical response to GCR is shown in the right panels of Fig. 5 and Fig. 6, respectively. Due to the low altitude and broader latitude span of GCR energy deposition, the ozone impact is quite different from aurora and SPEs. Since GCR peaks around 13 km with a significant tropospheric component, there is upwards of about 40% increase in NO_y and about a 15% increase in ozone in the troposphere.

EPP impact on the middle atmosphere

K. Semeniuk et al.

Title Page

Abstract

Introduction

Conclusions

References

Tables

Figures

◀

▶

◀

▶

Back

Close

Full Screen / Esc

Printer-friendly Version

Interactive Discussion



EPP impact on the middle atmosphere

K. Semeniuk et al.

[Title Page](#)[Abstract](#)[Introduction](#)[Conclusions](#)[References](#)[Tables](#)[Figures](#)[◀](#)[▶](#)[◀](#)[▶](#)[Back](#)[Close](#)[Full Screen / Esc](#)[Printer-friendly Version](#)[Interactive Discussion](#)

The ionization from GCR above 20 km is small, nevertheless there is a statistically significant ozone loss between the pole and 50° S in a roughly 5 km layer centered at 20 km in JJA. No such ozone loss occurs in the winter polar region in DJF, indicating the effect of a more disturbed vortex in the NH winter. However, in the SH summer there is ozone loss in the polar region between 25 and 30 km, which is associated with enhanced NO_x in this layer. The SH summer polar region exhibits dynamical variability around 20 km which obscures the chemical impact of GCR, much like in the SPEs case.

The situation in the lowermost stratosphere (between the tropopause and 20 km) is more complex since this is the region where the transition from ozone production to ozone loss for additional NO_x occurs (see above). There is poleward and downward transport in the stratosphere which pushes down the GCR induced ozone anomaly in the lowermost stratosphere and brings ozone depleted (number density) air from above 20 km. This transport effect can be seen in the difference in the altitude of the ozone increase between the two hemispheres. There is more diabatic descent in the Northern Hemisphere winter compared to the Southern Hemisphere winter (Andrews et al., 1987) so the region of ozone enhancement does not extend as high into the lowermost stratosphere.

There is a roughly 1% drop in ozone in middle and low latitudes between 20 and 30 km in both JJA and DJF where the GCR NO_x production acts to destroy ozone. As with the auroral and SPEs cases there is a loss of HO_x below 30 km due to interactions with NO_x and HNO₃. The difference in the SH middle and low latitude zonal wind change associated with GCR is likely due to the distribution of ozone reduction. The ozone loss around 20 km in the SH winter pole region gives rise to a vortex disturbance similar to the other two EPP cases. The loss of ozone between 20 and 30 km at lower latitudes is likely reducing the radiative equilibrium temperature gradient in this layer in fall and early winter and producing weaker westerlies at these latitudes during JJA (changes in the zonal wind due to thermal wind balance at one height propagate to all heights above). As discussed below this alters the Rossby wave transmission into the

SH leading to the hemispheric temperature and circulation changes seen in Fig. 4.

4.4 Combined EPP effect

For each of three EPP simulations conducted there is a reduction in the SH polar vortex strength and a warm temperature anomaly in the polar middle SH stratosphere, which satisfies thermal wind balance (Fig. 4). This is likely due to the decrease in ozone in the middle to high latitudes between 20 km and 30 km. As a result, the meridional gradient of the radiative equilibrium temperature is reduced in the polar region from early winter. This modifies the evolution of the polar vortex, which is slightly weaker becoming more prone to Rossby wave penetration and hence additional wave drag (through radiative damping of Rossby waves directly and through redistribution of the wave breaking in the surf zone). The additional Rossby wave drag increases the Brewer-Dobson circulation in the SH winter, which acts to increase dynamical heating in the polar SH and gives rise to the polar warm temperature anomaly. However, it will become apparent in the next subsection that there are other response patterns to EPP which do not conform to this picture.

The timing of the ozone impact on the stratospheric circulation for GCR and SPEs is different from that of aurora since the latter depends on descent of NO_x from the upper mesosphere. In the case of aurora, the polar vortex and Brewer-Dobson circulation are modified when the polar vortex is established and there is downward descent from the mesosphere. For the continuously acting GCR ionization (as opposed to transport dependent auroral and intermittent SPEs cases) the ozone reduction in the stratosphere is present through all stages of polar vortex formation and this may explain why it produces a similar dynamical impact to aurora even though the ozone impact is weaker in the critical region between 20 km and 30 km. SPEs can occur at any time of the year so they can influence the vortex evolution from its early onset stage or when it is established, but the impact is large so that the run mean polar vortex response is not negligible. Based on previous work (Jackman et al., 2009) there is an ozone memory that extends the period of the SPEs impact.

EPP impact on the middle atmosphere

K. Semeniuk et al.

Title Page

Abstract

Introduction

Conclusions

References

Tables

Figures

◀

▶

◀

▶

Back

Close

Full Screen / Esc

Printer-friendly Version

Interactive Discussion



EPP impact on the middle atmosphere

K. Semeniuk et al.

[Title Page](#)[Abstract](#)[Introduction](#)[Conclusions](#)[References](#)[Tables](#)[Figures](#)[I◀](#)[▶I](#)[◀](#)[▶](#)[Back](#)[Close](#)[Full Screen / Esc](#)[Printer-friendly Version](#)[Interactive Discussion](#)

To assess the linearity of the addition of the individual EPP effects we compare differences from the reference run for the sum of the individual runs to a run with all three EPP types combined in Figs. 7 and 8. The combined impact on the chemical composition is essentially additive (Fig. 7). The dynamical response (Fig. 8) is not additive since the response for each of the individual EPP types is comparable to the response of all three combined. This results in the larger values in the left hand panels compared to the right hand panels in Fig. 8. It appears that the ozone reduction between 20 and 30 km is the common factor in the influence of the EPP types on SH polar vortex evolution. The three EPP types also act out of phase. GCR and SPEs are about 180° out of phase with each other and aurora is 90° out of phase with both (Fig. 2). This, together with the fact that the ozone perturbations are small, implies that the ozone reduction with all three types of EPP present is not different by large factor between 20 and 30 km. So the dynamical perturbation from the ozone loss in this region is comparable for each of the individual EPP simulations and the combined EPP simulation. It must be noted that the dynamical response to the ozone perturbations is nonlinear but saturates with a low amplitude based on the simulations presented here. The ozone perturbation from the combination of the three EPP types is not sufficiently large to drive the system out of this low amplitude regime.

4.5 Combined EPP ensemble run

In order to get a more quantitative estimate of the sensitivity of the middle atmosphere to EPP, two additional simulations with all three EPP types combined were produced giving a three member ensemble. The reference run was also extended into an ensemble with two more 28-year realizations. The results are shown in Figs. 9 and 10.

There is no longer a statistically significant wintertime zonal wind response in both hemispheres (Fig. 9, top panels). However, the zonal wind below 20 km and in the troposphere shows a statistically significant difference pattern identified by Polvani and Kushner (2002). They demonstrated using a mechanistic model that as the stratospheric polar vortex weakens, the subtropical jet moves equatorward. This

pattern was apparent in the runs for the individual EPP types as well. In the ensemble run, the SH polar vortex showed some degree of weakening below 30 km in all members.

The JJA SH temperature anomaly structure is different from the individual EPP run cases. It is colder between 20 and 40 km and warmer between 40 and 60 km. The individual EPP cases had a warming between 20 and 50 km with a cooling above. However, there is a significant warming between 5 and 15 km in the SH polar region that is associated with the weakening of the SH polar vortex above through thermal wind balance. The Brewer-Dobson circulation undergoes an intensification in the lowermost SH stratosphere which is consistent with the temperature increase. But between 20 and 40 km the Brewer-Dobson circulation weakens at the pole and in middle latitudes. This behaviour is similar to the SPEs case (Fig. 9, lower middle panel).

In contrast to the dynamical response, the chemical response is statistically significant and consists of a super-position of the chemical patterns from each of the individual EPP types (Fig. 10). This is consistent with the linearity test from Sect. 4.4.

The combined effect of the three particle precipitation types does not increase the significance level since there is not a unique response pattern in the middle atmosphere. A comparison of two of the combined EPP ensemble members for JJA is presented in Figs. 11 and 12, showing differences from the ensemble mean reference run. The SH middle atmosphere can respond to combined EPP forcing either through a weakening of the polar vortex, associated with a warming in the polar stratosphere, and more intense Brewer-Dobson circulation (Fig. 11, top panels), or vice versa (Fig. 11, bottom panels). However, the strong vortex case has a rather complicated structure with a weakening of the vortex closer to the pole between 20 and 40 km. This results in a similar zonal wind anomaly pattern for both cases between the surface and 20 km and in agreement with the findings of Polvani and Kushner (2002).

There are differences in the ozone field (Fig. 12, bottom panels), for the case with a weakened polar vortex (left panel) compared to the strengthened polar vortex case (right panel). Higher ozone values are present between 30 and 50 km in middle and

EPP impact on the middle atmosphere

K. Semeniuk et al.

Title Page

Abstract

Introduction

Conclusions

References

Tables

Figures

◀

▶

◀

▶

Back

Close

Full Screen / Esc

Printer-friendly Version

Interactive Discussion



low latitudes for the weakened polar vortex case. The two vortex regimes differentiate starting in May (not shown). The differences in the ozone field are not particularly striking, which implies that the divergence in the evolution is subtle. However, the results change when the solar cycle in irradiance is included, as addressed in the next section.

5 Combined solar variability and EPP ensemble runs

Here we present results of ensemble simulations which include the solar irradiance cycle. Two ensembles of three members each with and without combined EPP were produced. Each ensemble member was 28 years in duration using the same EPP forcings as the runs in the previous section. The ensemble with solar variability only is used as the reference ensemble for the following analysis instead of the reference ensemble used in Sect. 4 which lacks the solar irradiance cycle.

5.1 Long-term differences between the ensemble runs

The dynamical run mean, ensemble mean difference between the reference ensemble average and EPP ensemble average is shown in Fig. 13. In JJA the Brewer-Dobson circulation intensifies in the SH middle and low latitudes between 25 and 40 km. This is associated with a cooling of about 0.25 K in the tropics over the same altitude range. By contrast, the Brewer-Dobson circulation weakens in the NH during DJF around 30 km and there is no longer any significant temperature response between 25 and 40 km in the tropics. The SH polar vortex undergoes a small intensification poleward of about 50° S as well as a reduction around 30° S. In DJF the zonal wind experiences an intensification around 30° N with less statistically significant reduction in the polar region. The age of air (Fig. 14) is reduced by over 1% in most of the stratosphere in both JJA and DJF, which indicates that there is an overall intensification of tropical upwelling due to EPP.

EPP impact on the middle atmosphere

K. Semeniuk et al.

Title Page

Abstract

Introduction

Conclusions

References

Tables

Figures

◀

▶

◀

▶

Back

Close

Full Screen / Esc

Printer-friendly Version

Interactive Discussion



EPP impact on the middle atmosphere

K. Semeniuk et al.

[Title Page](#)[Abstract](#)[Introduction](#)[Conclusions](#)[References](#)[Tables](#)[Figures](#)[I◀](#)[▶I](#)[◀](#)[▶](#)[Back](#)[Close](#)[Full Screen / Esc](#)[Printer-friendly Version](#)[Interactive Discussion](#)

The above response pattern of the dynamics differs from the case presented in Fig. 9. Without solar variability, the SH polar vortex weakens between 20 and 40 km in the presence of EPP and there is no cooling in the tropics in JJA. There is no statistically significant zonal wind response in the NH winter stratosphere as well. The difference in the Brewer-Dobson circulation is more striking in the annual mean (Fig. 15). In the presence of solar variability (top panels) there is a long term intensification in the SH, which is reflected in a weakening of the zonal wind. Due to EPP the age of air decreases by about 1.3% in the middle atmosphere with solar variability compared to 0.8% without (not shown). Thus, it can be inferred that the solar cycle changes the dynamical sensitivity of the atmosphere to EPP.

The NO_y , HO_x and ozone run mean, ensemble mean differences are shown in Fig. 16 and are very similar to the runs without the solar cycle discussed in Sect. 4 (compare Fig. 16 with Fig. 10). The solar cycle variation in the composition of the middle atmosphere is small, so the EPP perturbation is acting on a similar basic state.

The total column ozone difference (Fig. 17) shows a decrease up to 4% in the winter polar regions. In the NH, the ozone column reduction is concentrated between 60°E and 60°W , while in the SH the reduction occurs at all longitudes. This reflects the more zonally symmetric structure of the SH polar vortex. In the tropics, there is an increase of about 0.3%. The tropical increase is associated with GCR. The positive impact of GCR on total column ozone at high latitudes (not shown) is overwhelmed by the effect of aurora and SPEs. This can also be inferred from Figs. 5 and 6, which show significant reductions in polar ozone above 15 km.

5.2 Solar cycle regression analysis

To analyze the solar cycle effect for runs with and without EPP, we regress the results of the ensemble runs against the F10.7 index. Use of this index is motivated by the fact that previous studies have been based on it (e.g., Austin et al., 2008) and that it captures the overall evolution of the solar cycle. The Ap index is more appropriate for aurora as it reflects geomagnetic activity but it does not suit GCR or SPEs.

5.2.1 Latitude-altitude response

The F10.7 index regression coefficient for zonal mean temperature, ozone, zonal wind, TEM mass streamfunction, age of air and water vapour is shown in Figs. 18–19. Without EPP there is a warm temperature anomaly in the SH polar stratosphere with an associated reduction in the strength of the SH polar vortex (Fig. 18, top panels). The weaker vortex facilitates a Brewer-Dobson circulation increase (Fig. 18, top right) due to additional Rossby wave drag as argued above. The SH warm temperature anomaly appears to be due to the ozone buildup in this region (Fig. 19, top middle). The diabatic circulation increase is hemispheric in scale and results in increased tropical upwelling and some reduction in the age of air (Fig. 19, top left).

In contrast to the solar cycle only runs, inclusion of EPP leads to an increase in the age of air during solar maximum years when compared to solar minimum years (Fig. 19, bottom left). This is because during solar minimum years the Brewer-Dobson circulation is more intense than during solar maximum years for runs with EPP (Fig. 18, bottom right) due to the zonal wind response pattern in the SH. Even though there is a reduction of ozone in the SH stratosphere polar latitudes there is still an ozone increase at middle to high latitudes (Fig. 19, bottom middle). There is no longer a positive temperature anomaly poleward of 60° S below 45 km, in better agreement with observations (Keckhut et al., 2005). The ozone buildup without EPP modifies the evolution of the polar vortex so as to make it weaker around 60° S by reducing the meridional temperature gradient. In the presence of EPP there is much less ozone increase in the sub-polar latitude band and the SH polar vortex intensifies during solar maxima (Fig. 18, bottom left).

An interesting effect of inclusion of EPP is the formation of a region with weak ozone response to the solar cycle around 30 km near the equator (Fig. 19, bottom middle). This feature is present in observations (Soukharev and Hood, 2006), although in these simulations it is not as pronounced. Analysis of the diabatic vertical wind in the tropics (not shown) suggests that there is an increase in the tropical upwelling above 30 km

EPP impact on the middle atmosphere

K. Semeniuk et al.

Title Page

Abstract

Introduction

Conclusions

References

Tables

Figures

◀

▶

◀

▶

Back

Close

Full Screen / Esc

Printer-friendly Version

Interactive Discussion



during solar maxima which offsets the buildup of ozone at its mixing ratio peak, which is at 30 km. The enhanced vertical transport is associated with enhanced horizontal transport of ozone to middle latitudes, counteracting the increased photochemical production of ozone.

Another significant feature associated with EPP is the increase in H₂O around the tropopause level and in the lowermost stratosphere during solar maximum years (Fig. 19, bottom right). This is driven by the warming temperatures in the cold trap region (Fig. 18, bottom middle) in the EPP ensemble. Without EPP there is a cooling in the TTL (Fig. 18, top middle). The source of the TTL temperature variation with the solar cycle and EPP is the increased Brewer-Dobson circulation during solar minimum years. The presence of a positive ozone anomaly in the TTL region is consistent with reduced upwelling. Partly, this is related to the large, positive vertical gradient of ozone in this region. But also, vertical upwelling is associated with horizontal transport so a weakening of the Brewer-Dobson circulation reduces the loss of ozone to middle latitudes. The H₂O increase itself leads to additional radiative warming in the TTL. The relative warming of the TTL during solar maximum years is not associated with enhanced GCR ozone production since it is in the minimum stage of its cycle.

5.2.2 Temporal and spatial profiles

Here the two solar variability ensembles are compared for zonal and global mean total column ozone and tropical mean vertical profiles of the fields presented in the previous subsection.

The yearly variation of global mean total column ozone due to the solar cycle is shown in Fig. 20. EPP can offset some of the solar cycle variation, as seen during the solar maximum around 1990. It appears that enhanced activity of SPEs during this solar maximum (see Fig. 2, second panel) is responsible for reducing total column ozone amounts.

Figure 21 presents the zonal mean total column ozone variation with latitude. The high latitude effect of EPP is most apparent in the SH where the maximum in total

EPP impact on the middle atmosphere

K. Semeniuk et al.

Title Page

Abstract

Introduction

Conclusions

References

Tables

Figures

◀

▶

◀

▶

Back

Close

Full Screen / Esc

Printer-friendly Version

Interactive Discussion



column ozone variation is greatly reduced and agrees much better with ground based observations (Fioletov et al., 2002, latest data provided courtesy of V. Fioletov). In the NH the variation is underestimated in the model since the model NH polar vortex is too disturbed compared to the real atmosphere.

5 Figure 22 compares the ozone regression coefficient averaged from 25° S to 25° N for the two solar variability ensemble runs and satellite observations (McLinden et al., 2009). As noted above, the model has an ozone solar cycle response minimum around 30 km with EPP. It is not as deep as in the observations but similar to other models (Austin et al., 2008) even though we do not have SST variability, which is thought to be responsible for this feature. In spite of the fact that the direct effect of EPP on the tropics is limited due to the high latitude confinement of auroral and SPEs NO_x production, the polar vortex perturbations have a global Brewer-Dobson circulation impact that acts to magnify the tropical signal of EPP.

10 The difference between the two ensembles is highlighted further in Fig. 23. EPP increases the temperature in the stratosphere tropics due to the reduction in the strength of the Brewer-Dobson circulation during solar maxima relative to solar minima. This leads to an increase in the age of air. The warming of the TTL in the EPP ensemble results in an increase in the water vapour entering the stratosphere.

15 The tropical mean age of air does not show any significant solar cycle dependence in the ensemble without EPP. This differs from the results shown in Fig. 14 of Austin et al. (2008). The solar variability without EPP ensemble had two members opposing the third giving an insignificant response in the mean. It is possible that three ensemble members is not enough but at the same time this different behaviour between ensemble members indicates that the dynamical response is not unique. This may not be the case if observed or interactive SSTs were used in the model, in which case they may force the middle atmosphere into a response pattern where the age of air increases from solar minimum to solar maximum.

20 The inclusion of the solar cycle in the models analyzed by Austin et al. (2008) did not result in any systematic increase in water vapour variation below 20 km (see their

EPP impact on the middle atmosphere

K. Semeniuk et al.

[Title Page](#)[Abstract](#)[Introduction](#)[Conclusions](#)[References](#)[Tables](#)[Figures](#)[◀](#)[▶](#)[◀](#)[▶](#)[Back](#)[Close](#)[Full Screen / Esc](#)[Printer-friendly Version](#)[Interactive Discussion](#)

Fig. 13) as in our results. The only model with upper atmosphere EPP included in addition to the solar cycle, WACCM (Marsh et al., 2007), did reach about 1.5% per 100 units F10.7 at 20 km.

The solar cycle variation of tropical stratosphere temperature improves with the addition of EPP compared to observations (Fig. 12 of Austin et al., 2008). In our simulations the temperature minimum around 30 km is absent without EPP and when it is included, the minimum is not as prominent as in models with QBO and variable SSTs. Comparing to observations, this suggests that tropical upwelling is not representing the atmospheric behaviour in many models that include either the QBO or variable SSTs or both. These models overestimate the ozone variation in this region so the deficiency is not purely radiative.

6 Discussion and conclusions

The results of our simulations show that addition of EPP to a chemistry climate model makes significant and persistent changes in the natural state of the middle atmosphere. In particular, both aurora and SPEs produce annual mean reductions of ozone in the polar regions of the stratosphere in the 3–10% range depending on location. This is in spite of the fact that auroral ionization peaks above 70 km and SPEs are very intermittent and is consistent with the results of previous studies (Callis et al., 1996; Jackman et al., 2009). There is comparable ozone loss in winter and summer in the polar regions between 20 and 30 km. The NO_y produced by EPP survives following the break up of the polar vortex (Orsolini et al., 2003) and continues to destroy ozone catalytically. GCR induces a 1% ozone loss in middle latitudes between 20 and 30 km in addition to indirect ozone loss in this region due to transport of ozone depleted air in the polar vortices and mixing into lower latitudes. These chemical effects of EPP translate into dynamical effects due to the importance of ozone for radiative transfer.

GCR increases NO_y by over 10% in the lowermost stratosphere. The NO_y of CMAM and other models in this region is lower than in observations (Brohede et al., 2008). So

EPP impact on the middle atmosphere

K. Semeniuk et al.

Title Page

Abstract

Introduction

Conclusions

References

Tables

Figures

◀

▶

◀

▶

Back

Close

Full Screen / Esc

Printer-friendly Version

Interactive Discussion



this EPP source together with aurora and SPEs helps to explain part of the deficit.

The long-term mean effect of EPP in the simulations with transient solar forcing presented here is to increase the Brewer-Dobson circulation and tropical upwelling. This reduces the age of air by 1 to 2% in the middle and upper stratosphere. The Brewer-Dobson circulation response varies with the solar cycle; it is weaker during solar maximum years compared to solar minimum years. This behaviour is tied to the EPP modification of the polar vortices through the change in high latitude ozone and hence the radiative equilibrium temperature around the terminator. A reduced meridional gradient of the radiative equilibrium temperature in the 60° to 80° latitude region leads to a slightly weaker polar vortex and hence more Rossby wave penetration which can be explained by the Charney-Drazin criterion (Andrews et al., 1987). This results in more Rossby wave drag in the stratosphere (especially the SH) and thus a stronger Brewer-Dobson circulation. However, the details of this process are subtle and the simulations with combined EPP excluding the solar cycle (Sect. 4) show that the dynamical response can be in the opposite sense as well (weaker Brewer-Dobson circulation and stronger polar vortex).

The regression analysis shows that EPP has a significant impact on the SH zonal wind variation with the solar cycle. Without EPP the zonal wind becomes weaker during solar maximum years, which does not fit in the idealized picture of Kodera and Kuroda (2002). EPP removes this disagreement. In the NH, the EPP does not alter the basic response of the polar vortex to the solar cycle in the model since it is in a more disturbed regime compared to the SH and the impact of EPP on the ozone evolution in the NH is weaker.

There is a Brewer-Dobson circulation reduction during solar maximum years compared to solar minimum years due to the intensification of the polar vortices and reduced Rossby wave penetration and associated drag in line with the idealized picture of Kodera and Kuroda (2002). As a result, there is a tropical temperature increase which results from reduced upwelling, and hence reduced adiabatic cooling, in the TTL. The cold trap warms during solar maxima which then leads to extra H₂O in the

EPP impact on the middle atmosphere

K. Semeniuk et al.

Title Page

Abstract

Introduction

Conclusions

References

Tables

Figures

◀

▶

◀

▶

Back

Close

Full Screen / Esc

Printer-friendly Version

Interactive Discussion



tropopause and lowermost stratosphere (up to 4%). Analysis of the tropical tropopause height based on the cold point diagnostic (not shown) indicates that there is no significant change in height due to EPP, specifically GCR and its associated ozone increase of about 15% in the troposphere. So tropopause height is not playing a role in the water vapour variation.

The H₂O variation in the TTL region and the lowermost stratosphere will have an effect on the surface temperature through radiative forcing (Solomon et al., 2010). This water vapour variation just above the tropopause may be an additional driver for the solar response at the surface. However, an explicit evaluation would require simulations with an interactive ocean. To the best of our knowledge, this mechanism has not been suggested before. It is not significant without EPP. This mechanism can affect decadal surface temperature trends reflecting variations in the solar cycle.

A significant feature of these results is that high latitude changes in Rossby wave drag are associated with tropical circulation changes. This can be seen in the pole to pole change in the age of air. However, the tropical response cannot be explained simply by the non-local nature of the diabatic streamfunction (Eliassen, 1951). Some of the low latitude Brewer-Dobson circulation variation from solar minima to solar maxima is due to Rossby wave propagation changes induced by variation of the polar vortices. But there are also sources associated with the subtropical jets such as synoptic scale Rossby waves and mountain wave drag (McLandress and Shepherd, 2009). There is a localized change of Eliassen-Palm flux divergence in the TTL which contributes to the solar cycle variation in temperature (not shown). Detailed analysis of this feature are beyond the scope of this paper.

Variation of TTL temperatures is also induced by interannual variation of SSTs (Schmidt, 2010) an effect which is not included in this study. SSTs change the tropopause height as well as the forcing of planetary Rossby waves so they can significantly influence the middle atmosphere circulation (see Rind et al., 2008, and references therein). Our results show that EPP has a non-negligible impact as well.

EPP impact on the middle atmosphere

K. Semeniuk et al.

Title Page

Abstract

Introduction

Conclusions

References

Tables

Figures

◀

▶

◀

▶

Back

Close

Full Screen / Esc

Printer-friendly Version

Interactive Discussion



Acknowledgements. The authors would like to thank the Natural Sciences and Engineering Research Council of Canada, the Canadian Foundation for Climate and Atmospheric Sciences and the Canadian Space Agency for support. Computing for this work was supported by the Canadian Foundation for Infrastructure, the Canadian Space Agency and the Ontario Innovation Trust.

References

- Andrews, D. G., Holton, J. R., and Leovy, C. B.: Middle atmosphere dynamics, Academic Press, Toronto, 489 pp., 1987. 24866, 24867, 24874, 24884
- Austin, J., Tourpali, K., Rozanov, E., Akiyoshi, H., Bekki, S., Bodeker, G., Brühl, C., Butchart, N., Chipperfield, M., Deushi, M., Fomichev, V. I., Giorgetta, M. A., Gray, L., Kodera, K., Lott, F., Manzini, E., Marsh, D., Matthes, K., Nagashima, T., Shibata, K., Stolarski, R. S., Struthers, H., and Tian, W.: Coupled chemistry climate model simulations of the solar cycle in ozone and temperature, *J. Geophys. Res.*, 113, D11306, doi:10.1029/2007JD009391, 2008. 24857, 24865, 24879, 24882, 24883
- Barth, C. A., Mankoff, K. D., Balley, S. M., and Solomon, S. C.: Global observations of nitric oxide in the thermosphere, *J. Geophys. Res.*, 108, 1027, doi:10.1029/2002JA009458, 2003. 24856
- Bazilevskaya, G. A., Usoskin, I. G., Flückiger, E. O., Harrison, R. G., Desorgher, L., Bütkofer, R., Krainev, M. B., Makhmutov, V. S., Stozhkov, Y. I., Svirzhetskaya, A. K., Svirzhovsky, N. S., and Kovaltsov, G. A.: Cosmic ray induced ion production in the atmosphere, *Space Sci. Rev.*, 137, 149–173, doi:10.1007/s11214-008-9339-y, 2008. 24865
- Beagley, S. R., de Grandpré, J., Koshyk, J. N., McFarlane, N. A., and Shepherd, T. G.: Radiative-dynamical climatology of the first-generation Canadian Middle Atmosphere Model, *Atmos.-Ocean*, 35, 293–331, 1997. 24858
- Brasseur, G. P. and Solomon, S.: *Aeronomy of the middle atmosphere*, Springer, 644 pp., The Netherlands, 2005. 24869
- Brohede, S., McLinden, C. A., Haley, C. S., Jonsson, A. I., and Murtagh, D.: Odin stratospheric proxy NO_y measurements and climatology, *Atmos. Chem. Phys.*, 8, 5731–5754, doi:10.5194/acp-8-5731-2008, 2008. 24858, 24883

EPP impact on the middle atmosphere

K. Semeniuk et al.

Title Page

Abstract

Introduction

Conclusions

References

Tables

Figures

◀

▶

◀

▶

Back

Close

Full Screen / Esc

Printer-friendly Version

Interactive Discussion



EPP impact on the middle atmosphere

K. Semeniuk et al.

Title Page

Abstract

Introduction

Conclusions

References

Tables

Figures

◀

▶

◀

▶

Back

Close

Full Screen / Esc

Printer-friendly Version

Interactive Discussion



- Brown, R. R.: Electron precipitation in the auroral zone, *Space Sci. Rev.*, 5, 311–387, doi:10.1007/BF02653249, 1966. 24864
- Callis, L. B., Baker, D., Natarajan, M., Blake, J., Mewaldt, R., Selesnick, R., and Cummings, J.: A 2D model simulation of downward transport of NO_y into the stratosphere: Effects on the 1994 austral spring O₃ and NO_y, *Geophys. Res. Lett.*, 23, 1905–1908, doi:10.1029/96GL01788, 1996. 24855, 24883
- Callis, L. B., Natarajan, M., Lambeth, J. D., and Baker, D. N.: Solar atmospheric coupling by electrons (SOLACE) 2. Calculated stratospheric effects of precipitating electrons, 1978–1988, *J. Geophys. Res.*, 103, 28,421–28,438, doi:10.1029/98JD02407, 1998. 24863
- Callis, L. B., Natarajan, M., and Lambeth, J. D.: Solar-atmosphere coupling by electrons (SOLACE): 3. Comparisons of simulations and observations, 1979–1997, issues and implications, *J. Geophys. Res.*, 106, 7523–7539, doi:10.1029/2000JD900615, 2001. 24855, 24857
- Crutzen, P. J., Isaksen, I. S. A., and Reid, G. C.: Solar proton events: Stratospheric sources of nitric oxide, *Science*, 189, 457–458, 1975. 24855
- de Grandpré, J., Sandilands, J. W., McConnell, J. C., Beagley, S. R., Croteau, P. C., and Danilin, M. Y.: Canadian Middle Atmosphere Model: preliminary results from the chemical transport module, *Atmos.-Ocean*, 35, 385–431, 1997. 24858
- de Grandpré, J., Beagley, S. R., Fomichev, V. I., Griffioen, E., McConnell, J. C., and Medvedev, A. S.: Ozone climatology using interactive chemistry: Results from the Canadian Middle Atmosphere Model, *J. Geophys. Res.*, 105, 26,475–26,491, doi:10.1029/2000JD900427, 2000. 24858
- Egorova, T., Rozanov, E., Manzini, E., Haberreiter, M., Schmutz, W., Zubov, V., and Peter, T.: Chemical and dynamical response to the 11-year variability of the solar irradiance simulated with a chemistry-climate model, *Geophys. Res. Lett.*, 31, L06119, doi:10.1029/2003GL019294, 2004. 24859
- Eliassen, A.: Slow thermally or frictionally controlled meridional circulation in a circular vortex, *Astrophys. Norv.*, 5, 19–60, 1951. 24885
- Eyring, V. et al.: Multimodel projections of stratospheric ozone in the 21st century, *J. Geophys. Res.*, 112, D16303, doi:10.1029/2006JD008332, 2007. 24858
- Feldstein, Y. I.: On morphology and auroral and magnetic disturbances at high latitudes, *Geomagn. Aeron.*, 3, 227–239, 1963. 24863
- Fioletov, V. E., Bodeker, G. E., Miller, A. J., McPeters, R. D., and Stolarski, R.: Global and zonal total ozone variations estimated from groundbased and satellite measurements: 1964–2000,

EPP impact on the middle atmosphere

K. Semeniuk et al.

Title Page

Abstract

Introduction

Conclusions

References

Tables

Figures

◀

▶

◀

▶

Back

Close

Full Screen / Esc

Printer-friendly Version

Interactive Discussion



J. Geophys. Res., 107, 4647, doi:10.1029/2001JD001350, 2002. 24882, 24915

Fomichev, V. I.: The radiative energy budget of the middle atmosphere and its parameterizations in general circulation models., J. Atmos. Solar Terr. Phys., 71, 1577–1585, doi:10.1016/j.jastp.2009.04.007, 2009. 24859

5 Fomichev, V. I., Fu, C., de Grandpré, J., Beagley, S. R., Ogibalov, V. P., and McConnell, J. C.: Model thermal response to minor radiative energy sources and sinks in the middle atmosphere, J. Geophys. Res., 109, D19107, doi:10.1029/2004JD004892, 2004. 24858

Fomichev, V. I., Forster, P. M., and Coauthors: Chapter 3: Radiation, in: SPARC CCMVal Report on the Evaluation of Chemistry-Climate Models, edited by Eyring, V., Shepherd, T. G., and Waugh, D. W., SPARC, Toronto, Ontario, Canada, Tech. Rep. WCRP-132/WMO/TD-1526/SPARC Rep. 5, 2010. 24860

Fröhlich, C. and Lean, J.: Solar radiative output and its variability: evidence and mechanisms, Astron. Astrophys. Rev., 12, 273–320, doi:10.1007/s00159-004-0024-1, 2004. 24859

10 Gledhill, J. A.: The range-energy relation for 0.1–600 keV electrons, J. Phys. A: Math, Nucl. Gen., 6, 1420–1428, 1973. 24863

Hamill, P., Brogniez, C., and Coauthors: Chapter 4: Stratospheric aerosol record and climatology, in: Assessment of Stratospheric Aerosol Properties (ASAP), edited by: Thomason, L. and Peter, T., 107–176, SPARC, Toronto, Ontario, Canada, Tech. Rep. WCRP-124/WMO/TD-1295/SPARC Rep. 4, 2006. 24866

20 Hauchecorne, A., Bertaux, J.-L., Dalaudier, F., Cot, C., Lebrun, J.-C., Bekki, S., Marchand, M., Kyrölä, E., Tamminen, J., Sofieva, V., Fussen, D., Vanhellemont, F., d'Andon, O. F., Barrot, G., Mangin, A., Théodore, B., Guirlet, M., Snoeij, P., Koopman, R., de Miguel, L. S., Fraisse, R., and Renard, J.-B.: First simultaneous global measurements of nighttime stratospheric NO₂ and NO₃ observed by Global Ozone Monitoring by Occultation of Stars (GOMOS)/Envisat in 2003, J. Geophys. Res., 110, D18301, doi:10.1029/2004JD005711, 2005. 24856

25 Hauchecorne, A., Bertaux, J.-L., Dalaudier, F., Russell III, J. M., Mlynczak, M. G., Kyrölä, E., and Fussen, D.: Large increase of NO₂ in the north polar mesosphere in January–February 2004: Evidence of a dynamical origin from GOMOS/ENVISAT and SABER/TIMED data, Geophys. Res. Lett., 34, L03810, doi:10.1029/2006GL027628, 2007. 24856, 24858

30 Heaps, M.: Parameterization of the cosmic ray ion-pair production rate above 18 km, Planet Space Sci., 26, 513–517, 1978. 24856

Holzworth, R. H. and Meng, C.-I.: Mathematical representation of the auroral oval, Geophys. Res. Lett., 2, 377–380, doi:10.1029/GL002i009p00377, 1975. 24863, 24864

EPP impact on the middle atmosphere

K. Semeniuk et al.

Title Page

Abstract

Introduction

Conclusions

References

Tables

Figures

◀

▶

◀

▶

Back

Close

Full Screen / Esc

Printer-friendly Version

Interactive Discussion



Huang, T. Y. W., Brasseur, G. P., and Coauthors: Description of the SOCRATES – A chemical dynamical radiative two-dimensional model., Tech. Rep. NCAR/TN-440+EDD, NCAR, Boulder, CO, 94 pp., 1998. 24856

IAGA/V-MOD website:<http://www.ngdc.noaa.gov/IAGA/vmod>, 2008. 24865

5 Jackman, C. H.: Ionization rates for 1963–2005 from solar proton events, http://www.geo.fu-berlin.de/en/met/ag/strat/forschung/SOLARIS/Input_data, unpublished technical note, 2006. 24864

10 Jackman, C. H., DeLand, M. T., Labow, G. J., Fleming, E. L., Weisenstein, D. K., Ko, M. K. W., Sinnhuber, M., Anderson, J., and Russell, J. M.: The influence of the several very large solar proton events in years 2000–2003 on the neutral middle atmosphere, *Adv. Space Res.*, 35, 445–450, 2005. 24856, 24862, 24864

15 Jackman, C. H., Marsh, D. R., Vitt, F. M., Garcia, R. R., Fleming, E. L., Labow, G. J., Randall, C. E., López-Puertas, M., Funke, B., von Clarmann, T., and Stiller, G. P.: Short and medium-term atmospheric constituent effects of very large solar proton events, *Atmos. Chem. Phys.*, 8, 765–785, doi:10.5194/acp-8-765-2008, 2008. 24856

20 Jackman, C. H., Marsh, D. R., Vitt, F. M., Garcia, R. R., Randall, C. E., Fleming, E. L., and Frith, S. M.: Long-term middle atmosphere influence of very large solar proton events, *J. Geophys. Res.*, 114, D11304, doi:10.1029/2008JD011415, 2009. 24875, 24883

25 Keckhut, P., Cagnazzo, C., Chanin, M.-L., Claud, C., and Hauchecorne, A.: The 11-year solar-cycle effects on the temperature in the upper-stratosphere and mesosphere: Part I – Assessment of observations, *J. Atmos. Sol.-Terr. Phys.*, 67, doi:10.1016/j.jastp.2005.01.008, 2005. 24880

Kodera, K. and Kuroda, Y.: Dynamical response to the solar cycle, *J. Geophys. Res.*, 107, 4749, doi:10.1029/2002JD002224, 2002. 24855, 24884

30 Kodera, K. and Shibata, K.: Solar influence on the tropical stratosphere and troposphere in the northern summer, *Geophys. Res. Lett.*, 33, L19704, doi:10.1029/2006GL026659, 2006. 24855

Kodera, K., Hori, M. E., Yukimoto, S., and Sigmond, M.: Solar modulation of the Northern Hemisphere winter trends and its implications with increasing CO₂, *Geophys. Res. Lett.*, 35, L03704, doi:10.1029/2007GL031958, 2008. 24855

Kondrashov, D. and Ghil, M.: Spatio-temporal filling of missing points in geophysical data sets, *Nonlin. Processes Geophys.*, 13, 151–159, doi:10.5194/npg-13-151-2006, 2006. 24862

Kuroda, Y. and Kodera, K.: Effect of the solar cycle on the Polar-night jet oscillation, *J. Met.*

EPP impact on the middle atmosphere

K. Semeniuk et al.

Title Page

Abstract

Introduction

Conclusions

References

Tables

Figures

◀

▶

◀

▶

Back

Close

Full Screen / Esc

Printer-friendly Version

Interactive Discussion



Soc. Japan, 80, 973–984, 2002. 24855

López-Puertas, M., Funke, B., Gil-López, S., von Clarmann, T., Stiller, G. P., Hopfner, M., Kellmann, S., Fischer, H., and Jackman, C. H.: Observation of NO_x enhancement and ozone depletion in the Northern and Southern Hemispheres after the October–November 2003 solar proton events, *J. Geophys. Res.*, 110, A09S43, doi:10.1029/2005JA011050, 2005. 24856

Marsh, D. R., Garcia, R. R., Kinnison, D. E., Boville, B. A., Sassi, F., Solomon, S. C., and Matthes, K.: Modeling the whole atmosphere response to solar cycle changes in radiative and geomagnetic forcing, *J. Geophys. Res.*, 112, D23306, doi:10.1029/2006JD008306, 2007. 24856, 24883

McLandress, C. and Shepherd, T. G.: Impact of climate change on stratospheric sudden warmings as simulated by the Canadian Middle Atmosphere Model, *J. Clim.*, 22, 5449–5463, doi:10.1175/2009JCLI3069.1, 2009. 24858, 24885

McLinden, C. A., Tegtmeier, S., and Fioletov, V.: Technical Note: A SAGE-corrected SBUV zonal-mean ozone data set, *Atmos. Chem. Phys.*, 9, 7963–7972, doi:10.5194/acp-9-7963-2009, 2009. 24882, 24916

Melo, S. M. L., Blatherwick, R., Davies, J., Fogal, P., de Grandpré, J., McConnell, J. C., McElroy, C. T., McLandress, C., Murcray, F. J., Olson, J. R., Semeniuk, K., Shepherd, T. G., Strong, K., Tarasick, D., and Williams-Rioux, B. J.: Summertime stratospheric processes at northern mid-latitudes: comparisons between MANTRA balloon measurements and the Canadian Middle Atmosphere Model, *Atmos. Chem. Phys.*, 8, 2057–2071, doi:10.5194/acp-8-2057-2008, 2008. 24858

Nissen, K. M., Matthes, K., Langematz, U., and Mayer, B.: Towards a better representation of the solar cycle in general circulation models, *Atmos. Chem. Phys.*, 7, 5391–5400, doi:10.5194/acp-7-5391-2007, 2007. 24859

NOAA/POES website: <http://ngdc.noaa.gov/stp/satellite/poes/index.html>, 2008. 24862

Orsolini, Y. J., Eskes, H., Hansen, G., Hoppe, U.-P., Kylling, A., Kyrö, E., Notholt, J., Van der A, R., and von der Gathen, P.: Summertime low-ozone episodes at northern high latitudes, *Q. J. Roy. Met. Soc.*, 129, 3265–3275, doi:10.1256/qj.02.211, 2003. 24883

Polvani, L. M. and Kushner, P. J.: Tropospheric response to stratospheric perturbations in relatively simple general circulation model, *Geophys. Res. Lett.*, 29, 1114, doi:10.1029/2001GL014284, 2002. 24876, 24877

Porter, H. S., Jackman, C. H., and Green, A. E. S.: Efficiencies for production of atomic nitrogen and oxygen by relativistic proton impact in air, *J. Chem. Phys.*, 65, 154–167,

EPP impact on the middle atmosphere

K. Semeniuk et al.

Title Page

Abstract

Introduction

Conclusions

References

Tables

Figures

◀

▶

◀

▶

Back

Close

Full Screen / Esc

Printer-friendly Version

Interactive Discussion



doi:10.1063/1.432812, 1976. 24857, 24861

Randall, C., Rusch, D., Bevilacqua, R., Hoppel, K., and Lumpe, J.: Polar Ozone and Aerosol Measurement (POAM) II stratospheric NO₂, 1993–1996, *J. Geophys. Res.*, 103, 28,361–28,371, doi:10.1029/98JD02092, 1998. 24855

5 Randall, C. E., Siskind, D. E., and Bevilacqua, R. M.: Stratospheric NO_x enhancement in the Southern Hemisphere vortex in winter/spring of 2000, *Geophys. Res. Lett.*, 28, 2385–2388, doi:10.1029/2000GL012746, 2001. 24855, 24856

Randall, C. E., Harvey, V. L., Manney, G. L., Orsolini, Y., Codrescu, M., Sioris, C., Brohede, S., Haley, C. S., Gordley, L. L., Zawodny, J. M., and Russell III, J. M.: Stratospheric effects of energetic particle precipitation in 2003–2004, *Geophys. Res. Lett.*, 32, L05802, doi:10.1029/2004GL022003, 2005. 24856

Randall, C. E., Harvey, V. L., Siskind, D., France, J., Bernath, P., Boone, C., and Walker, K.: NO_x descent in the Arctic middle atmosphere in early 2009, *Geophys. Res. Lett.*, 36, L18811, doi:10.1029/2009GL039706, 2009. 24858

15 Randel, W. J. and Wu, F.: A stratospheric ozone profile data set for 1979–2005: Variability, trends, and comparisons with column ozone data, *J. Geophys. Res.*, 112, D06313, doi:10.1029/2006JD007339, 2007. 24866

Reddman, T., Ruhnke, R., Versick, S., and Kouker, W.: Modeling disturbed stratospheric chemistry during solar-induced NO_x enhancements observed with MIPAS/ENVISAT, *J. Geophys. Res.*, 115, D00I11, doi:10.1029/2009JD012569, 2010. 24856

20 Rees, M. H.: *Physics and chemistry of the upper atmosphere*, Cambridge University Press, Cambridge, UK, 289 pp., 1989. 24863

Rind, D., Lean, J., Lerner, J., Lonergan, P., and Leboissitier, A.: Exploring the stratospheric/tropospheric response to solar forcing, *J. Geophys. Res.*, 113, D24103, doi:10.1029/2008JD010114, 2008. 24855, 24885

25 Rinsland, C. P., Gunson, M. R., Salawitch, R. J., Newchurch, M. J., Zander, R., Abbas, M. M., Abrams, M. C., Manney, G. L., Michelsen, H. A., Chang, A. Y., and Goldman, A.: ATMOS measurements of H₂O + 2CH₄ and total reactive nitrogen in the November 1994 Antarctic stratosphere: Dehydration and denitrification in the vortex, *Geophys. Res. Lett.*, 23, 2397–2400, doi:10.1029/96GL00048, 1996. 24855

30 Rozanov, E., Callis, L., Schlesinger, M., Yang, F., Andronova, N., and Zubov, V.: Atmospheric response to NO_y source due to energetic electron precipitation, *Geophys. Res. Lett.*, 32, L14811, doi:10.1029/2005GL023041, 2005. 24856

EPP impact on the middle atmosphere

K. Semeniuk et al.

Title Page

Abstract

Introduction

Conclusions

References

Tables

Figures

◀

▶

◀

▶

Back

Close

Full Screen / Esc

Printer-friendly Version

Interactive Discussion



Russell, J. M., Solomon, S., Gordley, L. L., Remsberg, E. E., and Callis, L. B.: The variability of stratospheric and mesospheric NO₂ in the polar winter night observed by LIMS, *J. Geophys. Res.*, 89, 7267–7275, doi:10.1029/JD089iD05p07267, 1984. 24855

Schmidt, H.: Numerical simulation of the MLT response to natural and anthropogenic forcing for the period 1960 to 2006, The 6th IAGA/ICMA/CAWSES workshop on Long-Term Changes and Trends in the Atmosphere, NCAR, Boulder, Colorado, USA, 15–18 June, 2010. 24885

Schmidt, H., Brasseur, G. P., Charron, M., Manzini, E., Giorgetta, M. A., Diehl, T., Fomichev, V. I., Kinnison, D., Marsh, D., and Walters, S.: The HAMMONIA chemistry climate model: sensitivity to the mesopause region to the 11 years solar cycle and CO₂ doubling, *J. Clim.*, 19, 3903–3931, 2006. 24856

Seale, R. A. and Bushnell, R. H.: TIROS-N/NOAA A-J space environment monitor subsystem, NOAA technical memorandum ERL SEL/75, National Oceanic and Atmospheric Administration, Environmental Research Laboratories, Space Environment Laboratory, Boulder, Colorado, USA, 1987. 24862

Semeniuk, K., McConnell, J. C., Jin, J. J., Jarosz, J. R., Boone, C. D., and Bernath, P. F.: N₂O production by high energy auroral electron precipitation, *J. Geophys. Res.*, 113, D16302, doi:10.1029/2007JD009690, 2008. 24858

Shindell, D., Rind, D., Balachandran, N., Lean, J., and Lonergan, P.: Solar cycle variability, ozone, and climate, *Science*, 284, 305–308, doi:10.1126/science.284.5412.305, 1999. 24855

Siskind, D. E.: On the coupling between middle and upper atmospheric odd nitrogen, in: *Atmospheric Science Across the Stratopause*, Geophys. Monogr. Ser., vol. 123, edited by: Siskind, D. E., Eckermann, S. D., and Summers, M. E., 101–116, AGU, Washington, DC, USA, 2000. 24856

SOLARIS website: http://www.geo.fu-berlin.de/en/met/ag/strat/forschung/SOLARIS/Input_data, 2008. 24860

Solomon, S. and Crutzen, P. J.: Analysis of the August 1972 solar proton event including chlorine chemistry, *J. Geophys. Res.*, 86, 1140–1146, doi:10.1029/JC086iC02p01140, 1981. 24855, 24857, 24861

Solomon, S., Rusch, D. W., Gerard, J. C., Reid, G. C., and Crutzen, P. J.: The effect of particle precipitation events on the neutral and ion chemistry of the middle atmosphere, 2, *Odd hydrogen*, *Planet. Space Sci.*, 29, 885–893, doi:10.1016/0032-0633(81)90078-7, 1981. 24855

Solomon, S., Rosenlof, K. H., Portmann, R. W., Daniel, J. S., Davis, S. M., Sanford, T. J., and

EPP impact on the middle atmosphere

K. Semeniuk et al.

[Title Page](#)[Abstract](#)[Introduction](#)[Conclusions](#)[References](#)[Tables](#)[Figures](#)[◀](#)[▶](#)[◀](#)[▶](#)[Back](#)[Close](#)[Full Screen / Esc](#)[Printer-friendly Version](#)[Interactive Discussion](#)

- Plattner, G.-K.: Contributions of stratospheric water vapor to decadal changes in the rate of global warming, *Science*, 327, 1219–1223, doi:10.1126/science.1182488, 2010. 24885
- Soukharev, B. E. and Hood, L. L.: Solar cycle variation of stratospheric ozone: Multiple regression analysis of long-term satellite data sets and comparison with models, *J. Geophys. Res.*, 111, D20314, doi:10.1029/2006JD007107, 2006. 24880
- 5 Starkov, G. V.: Statistical dependences between the magnetic activity indices, *Geomagn. Aeronomy*, 34, 101–103, 1994. 24864
- Stiller, G. P., Tsidu, G. M., von Clarmann, T., Glatthor, N., Höpfner, M., Kellman, S., Linden, A., Ruhnke, R., Fischer, H., López-Puertas, M., Funke, B., and Gil-López, S.: An enhanced HNO₃ second maximum in the Antarctic midwinter upper stratosphere 2003, *J. Geophys. Res.*, 110, D20303, doi:10.1029/2005JD006011, 2005. 24862
- 10 Swider, W. and Keneshea, T. J.: Decrease of ozone and atomic oxygen in the lower mesosphere during a PCA event, *Planet. Space Sci.*, 21, 1969–1973, doi:10.1016/0032-0633(73)90126-8, 1973. 24855
- 15 Tiao, G. C., Reinsel, G. C., Xu, D., Pedrick, J. H., Zhu, X., Miller, A. J., DeLuisi, J. J., Mateer, C. L., and Wuebbles, D. J.: Effects of autocorrelation and temporal sampling schemes on estimates of trend and spatial correlation, *J. Geophys. Res.*, 95, 20,507–20,517, doi:10.1029/JD095iD12p20507, 1990. 24865
- Tsyganenko, N. A., Usmanov, A. V., Papitashvili, V. O., Papitashvili, N. E., and Popov, V.: Software for computations of geomagnetic field and related coordinate systems, Special report, Soviet Geophysical Committee, Moscow, USSR, 58 pp., 1987. 24864
- 20 Usoskin, I. G. and Kovaltsov, G. A.: Cosmic ray induced ionization in the atmosphere: Full modeling and practical applications, *J. Geophys. Res.*, 111, D21206, doi:10.1029/2006JD007150, 2006. 24857, 24864
- 25 Usoskin, I. G., Alanko-Huotari, K., Kovaltsov, G. A., and Mursula, K.: Hemispheric modulation of cosmic rays: monthly reconstruction for 1951–2004, *J. Geophys. Res.*, 110, A12108, doi:10.1029/2005JA011250, 2005. 24865
- Usoskin, I. G., Kovaltsov, G. A., and Mironova, I. A.: Cosmic ray induced ionization model CRAC:CRIL: An extension to the upper atmosphere, *J. Geophys. Res.*, 115, D10302, doi:10.1029/2009JD013142, 2010. 24864
- 30 Verronen, P. T., Seppälä, A., Kyrölä, E., Tamminen, J., Pickett, H. M., and Turunen, E.: Production of odd hydrogen in the mesosphere during the January 2005 solar proton event, *J. Geophys. Res. Lett.*, 33, L24811, doi:10.1029/2006GL028115, 2006. 24862

- Warneck, P.: Cosmic radiation as a source of odd nitrogen in the stratosphere, *J. Geophys. Res.*, 77, 6589–6591, doi:10.1029/JC077i033p06589, 1972. 24855
WDC website: <http://wdc.kugi.kyoto-u.ac.jp>, 2008. 24864
- 5 White, W. B.: Response of tropical global ocean temperature to the Sun's quasi-decadal UV radiative forcing of the stratosphere, *J. Geophys. Res.*, 111, C09020, doi:10.1029/2004JC002552, 2006. 24854
- White, W. B., Lean, J., Cayan, D. R., and Dettinger, M. D.: Response of global upper ocean temperature to changing solar irradiance, *J. Geophys. Res.*, 102, 3255–3266, doi:10.1029/96JC03549, 1997. 24854
- 10 Wolter, K. and Timlin, M. S.: Measuring the strength of ENSO events: How does 1997/98 rank?, *Weather*, 53, 315–324, 1998. 24866

EPP impact on the middle atmosphere

K. Semeniuk et al.

Title Page

Abstract

Introduction

Conclusions

References

Tables

Figures

I◀

▶I

◀

▶

Back

Close

Full Screen / Esc

Printer-friendly Version

Interactive Discussion



EPP impact on the middle atmosphere

K. Semeniuk et al.

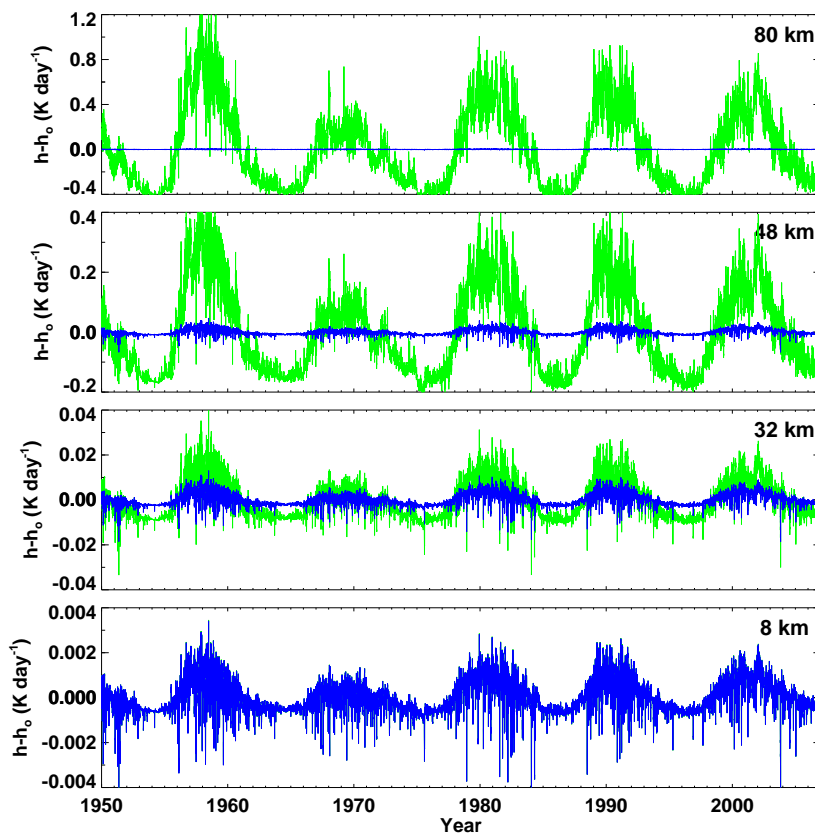


Fig. 1. Time series of the solar heating rate deviation from the 1950–2006 mean values in the troposphere (8 km), stratosphere (32 km), near the stratopause (48 km) and in the mesosphere (80 km). Blue: variability only in TSI is taken into account; green: variability in SSI is taken into account. An overhead Sun and equatorial ozone profile are considered in calculating the solar heating rates.

[Title Page](#)[Abstract](#)[Introduction](#)[Conclusions](#)[References](#)[Tables](#)[Figures](#)[◀](#)[▶](#)[◀](#)[▶](#)[Back](#)[Close](#)[Full Screen / Esc](#)[Printer-friendly Version](#)[Interactive Discussion](#)

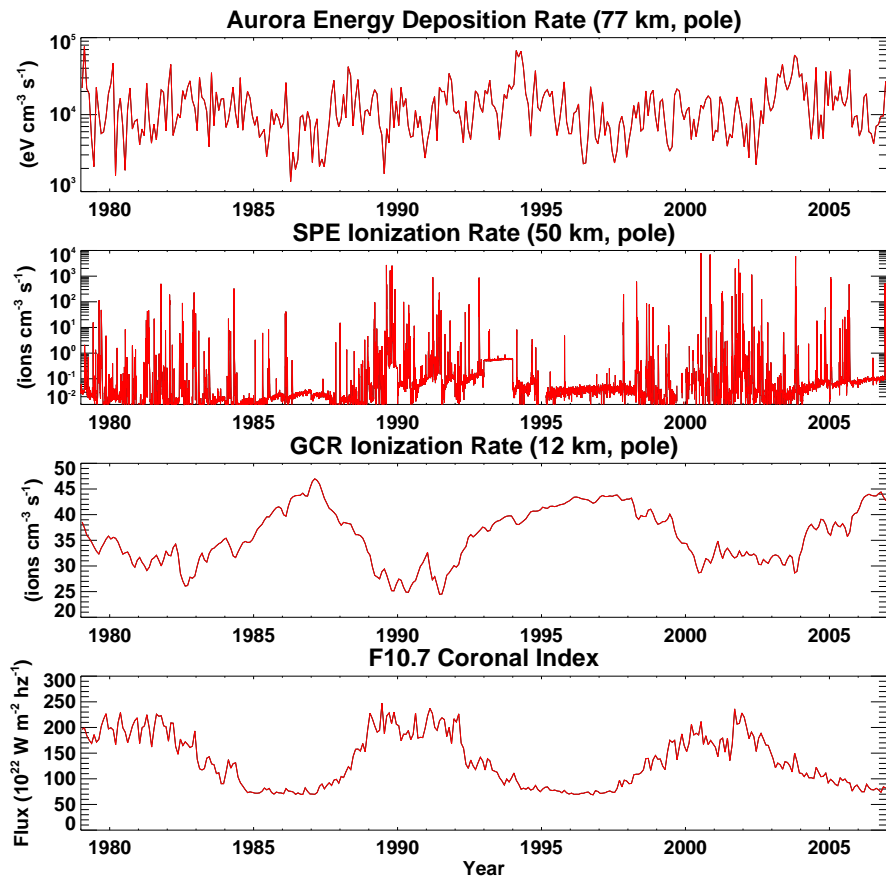


Fig. 2. Timeseries of energy deposition and ion pair production for aurora, SPEs and GCR. F10.7 variation is shown in the bottom panel.

EPP impact on the middle atmosphere

K. Semeniuk et al.

Title Page

Abstract Introduction

Conclusions References

Tables Figures

◀ ▶

◀ ▶

Back Close

Full Screen / Esc

Printer-friendly Version

Interactive Discussion



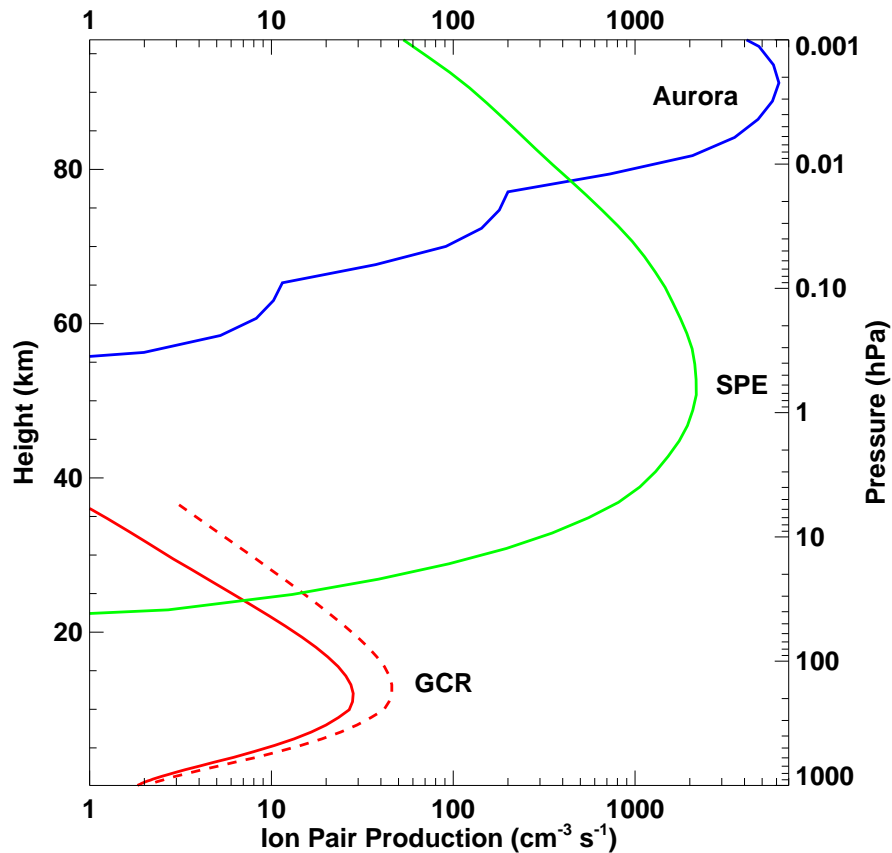


Fig. 3. Vertical profiles of the peak ion pair production rate for aurora (14 January 2004, blue), an SPE event (29 October 2003, green), and GCR (1991 minimum, red, and 1987 maximum, red dash).

EPP impact on the middle atmosphere

K. Semeniuk et al.

Title Page

Abstract Introduction

Conclusions References

Tables Figures

◀ ▶

◀ ▶

Back Close

Full Screen / Esc

Printer-friendly Version

Interactive Discussion



EPP impact on the middle atmosphere

K. Semeniuk et al.

Title Page

Abstract

Introduction

Conclusions

References

Tables

Figures

◀

▶

◀

▶

Back

Close

Full Screen / Esc

Printer-friendly Version

Interactive Discussion

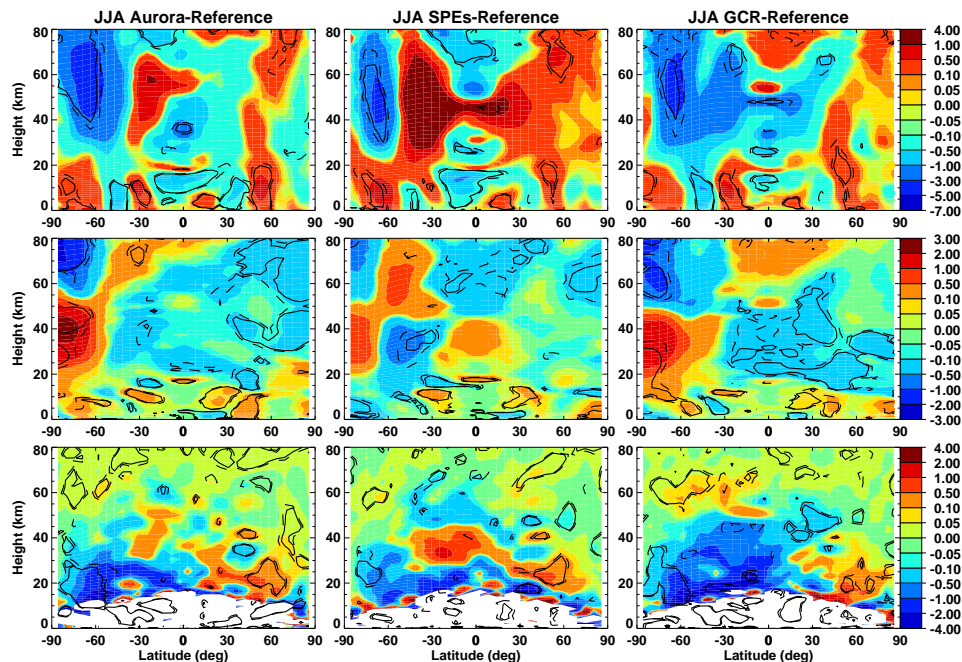


Fig. 4. Run mean, June–August mean differences compared to the reference run for aurora (left), SPEs (center) and GCR (right) showing zonal wind (top, m/s), temperature (middle, K) and mass streamfunction (bottom, kg/m/s, values outside the range (-4.4) not plotted). Solid and dashed contours denote regions with 95% and 90% confidence levels, respectively. These two contours are the same for all subsequent figures.

EPP impact on the middle atmosphere

K. Semeniuk et al.

Title Page

Abstract

Introduction

Conclusions

References

Tables

Figures

◀

▶

◀

▶

Back

Close

Full Screen / Esc

Printer-friendly Version

Interactive Discussion

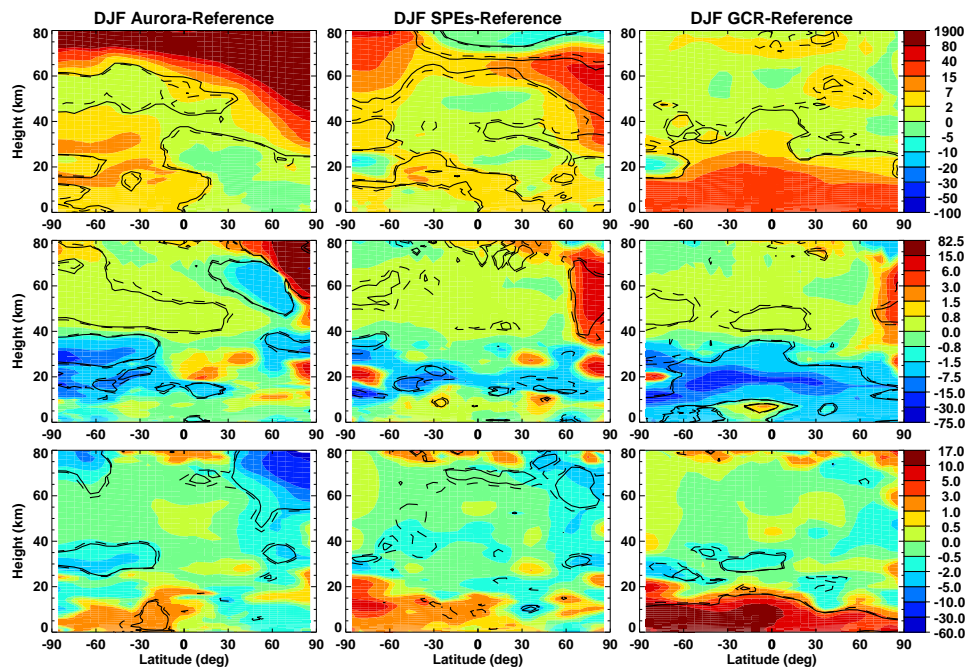


Fig. 5. Run mean, December–February mean NO_y (top), HO_x (middle) and O_3 (bottom) differences for aurora, SPEs and GCR runs compared to the reference run (%).

EPP impact on the middle atmosphere

K. Semeniuk et al.

Title Page

Abstract

Introduction

Conclusions

References

Tables

Figures

◀

▶

◀

▶

Back

Close

Full Screen / Esc

Printer-friendly Version

Interactive Discussion

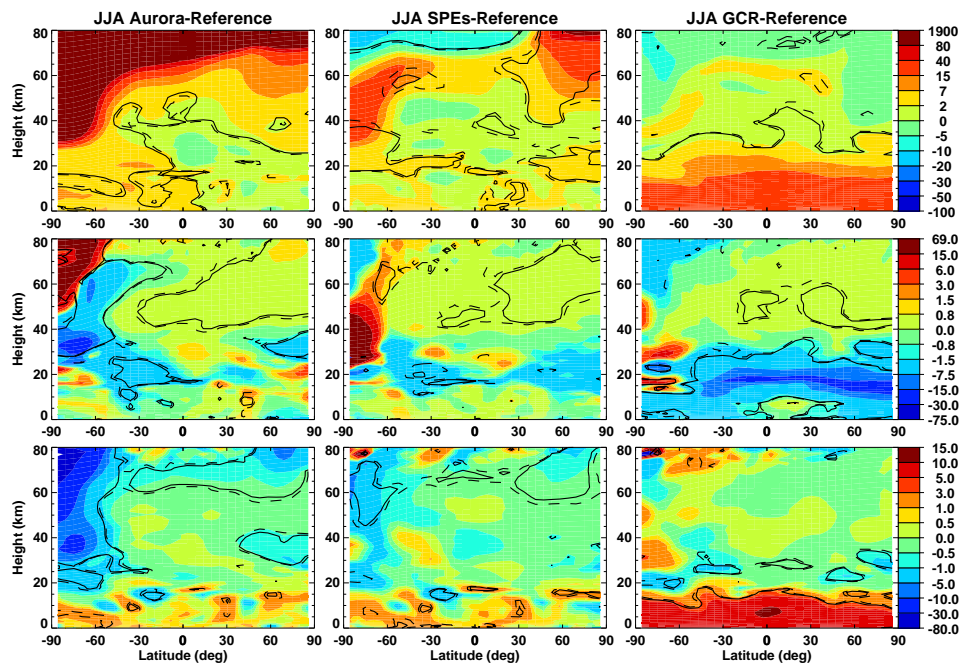


Fig. 6. Run mean, June–August mean compared to the reference run for aurora (left), SPEs (center) and GCR (right) showing NO_y (top), HO_x (middle) and O_3 (bottom) (%).

EPP impact on the middle atmosphere

K. Semeniuk et al.

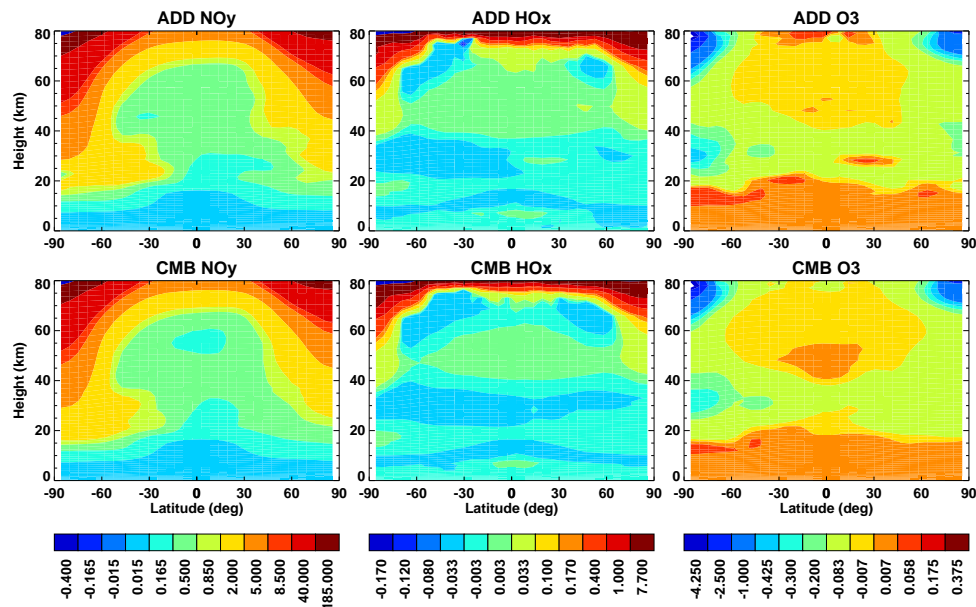


Fig. 7. Run mean, annual mean difference from the reference run for NO_y (left, ppbv), HO_x (middle, ppbv) and O_3 (right, ppmv). Top panels: sum for the individual aurora, SPEs and GCR runs. Bottom panels: combined run.

Title Page

Abstract

Introduction

Conclusions

References

Tables

Figures

◀

▶

◀

▶

Back

Close

Full Screen / Esc

Printer-friendly Version

Interactive Discussion



EPP impact on the middle atmosphere

K. Semeniuk et al.

Title Page

Abstract

Introduction

Conclusions

References

Tables

Figures

◀

▶

◀

▶

Back

Close

Full Screen / Esc

Printer-friendly Version

Interactive Discussion

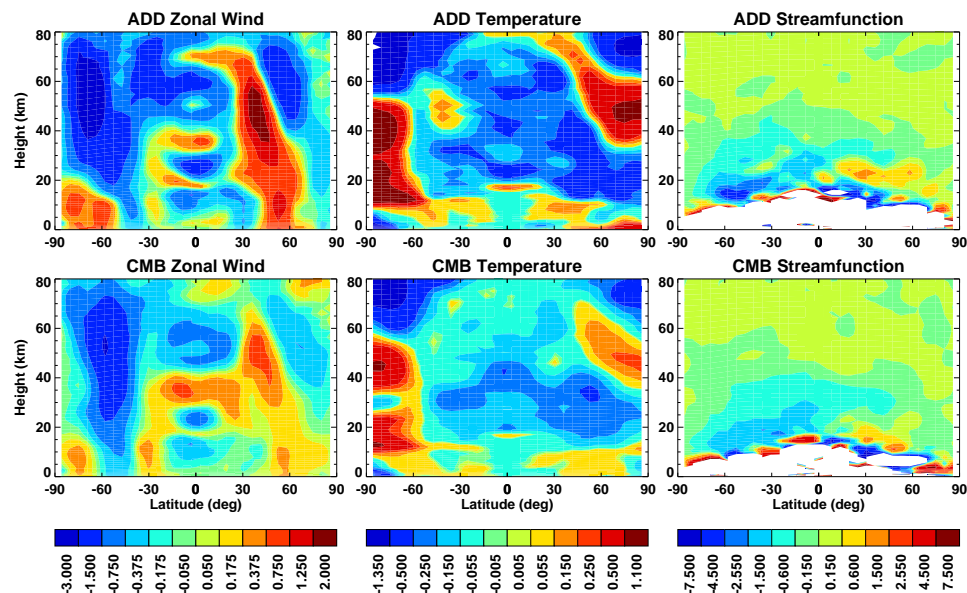


Fig. 8. Run mean, annual mean difference from the reference run for zonal wind (left), temperature (middle) and mass streamfunction (right, values outside the (-9.9) interval not plotted). Top panels: sum for the aurora, SPEs and GCR runs. Bottom panels: combined run.

EPP impact on the middle atmosphere

K. Semeniuk et al.

Title Page

Abstract

Introduction

Conclusions

References

Tables

Figures

◀

▶

◀

▶

Back

Close

Full Screen / Esc

Printer-friendly Version

Interactive Discussion

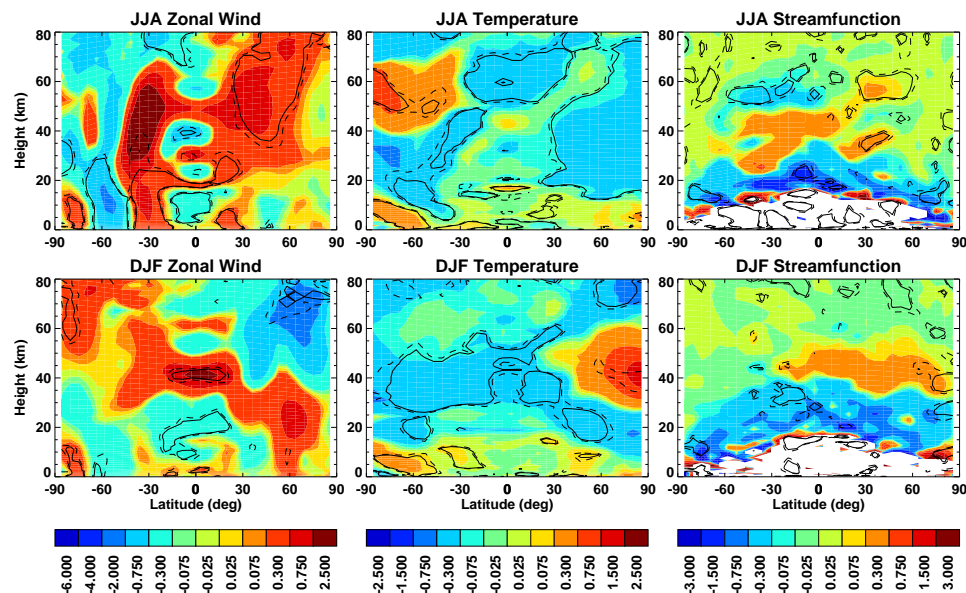


Fig. 9. June–August run mean, ensemble mean (top) and December–February run mean, ensemble mean (bottom) zonal wind (m/s), temperature (K), and mass streamfunction (kg/m², values outside the range (−4.4) not plotted) differences for the combined EPP ensemble run compared to the reference ensemble run.

EPP impact on the middle atmosphere

K. Semeniuk et al.

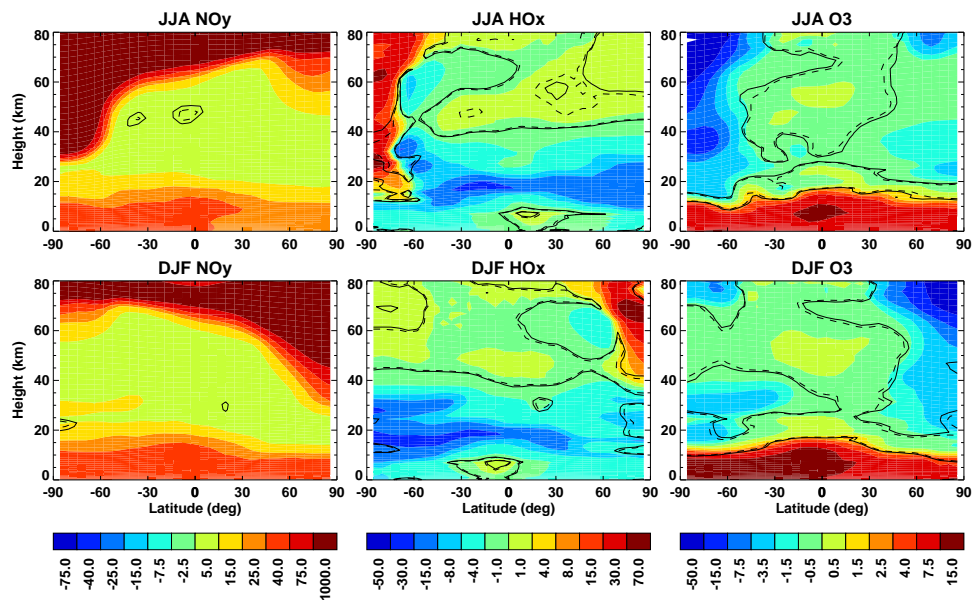


Fig. 10. June–August run mean, ensemble mean (top) and December–February run mean, ensemble mean (bottom) NO_y, HO_x and O₃ differences for the combined EPP ensemble run compared to reference ensemble run (%).

[Title Page](#)[Abstract](#)[Introduction](#)[Conclusions](#)[References](#)[Tables](#)[Figures](#)[◀](#)[▶](#)[◀](#)[▶](#)[Back](#)[Close](#)[Full Screen / Esc](#)[Printer-friendly Version](#)[Interactive Discussion](#)

EPP impact on the
middle atmosphere

K. Semeniuk et al.

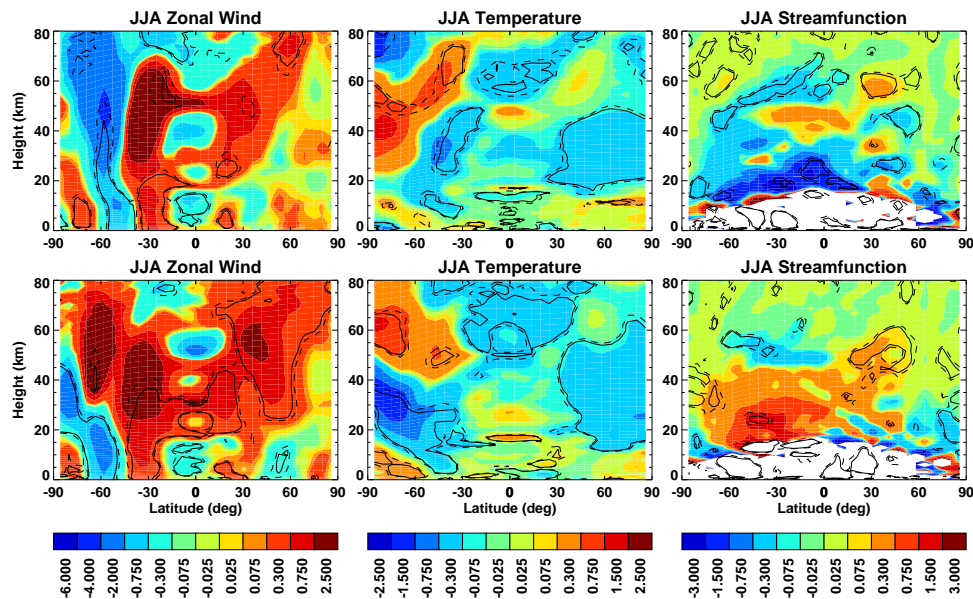


Fig. 11. June–August run mean difference of zonal wind, temperature and mass streamfunction from the ensemble reference run for two of the combined EPP ensemble members. Top, weak vortex case. Bottom, strong vortex case.

[Title Page](#)[Abstract](#)[Introduction](#)[Conclusions](#)[References](#)[Tables](#)[Figures](#)[◀](#)[▶](#)[◀](#)[▶](#)[Back](#)[Close](#)[Full Screen / Esc](#)[Printer-friendly Version](#)[Interactive Discussion](#)

EPP impact on the middle atmosphere

K. Semeniuk et al.

Title Page

Abstract

Introduction

Conclusions

References

Tables

Figures

◀

▶

◀

▶

Back

Close

Full Screen / Esc

Printer-friendly Version

Interactive Discussion

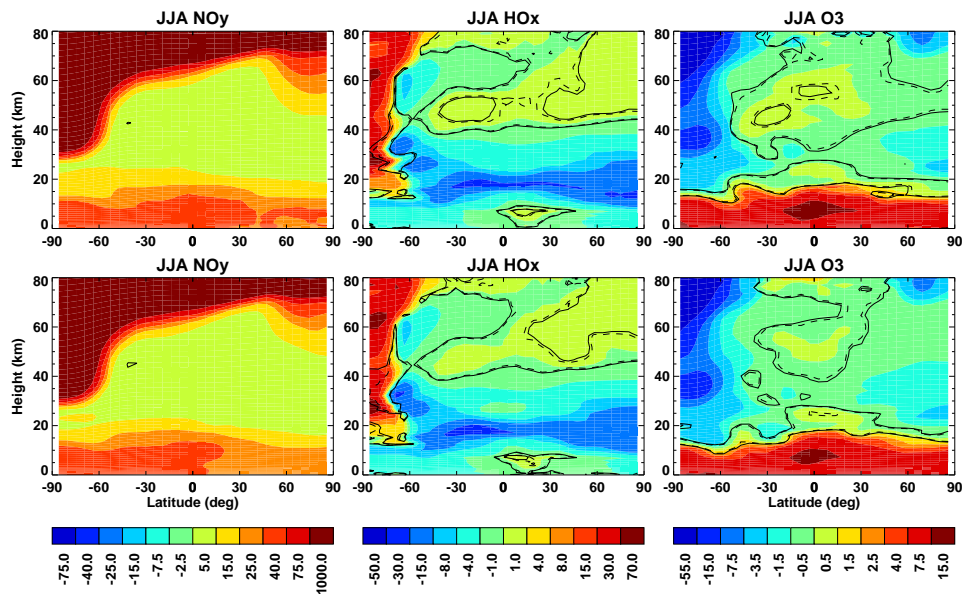


Fig. 12. As in Fig. 11 but for NO_y , HO_x and O_3 differences (%).

EPP impact on the middle atmosphere

K. Semeniuk et al.

Title Page

Abstract

Introduction

Conclusions

References

Tables

Figures

◀

▶

◀

▶

Back

Close

Full Screen / Esc

Printer-friendly Version

Interactive Discussion

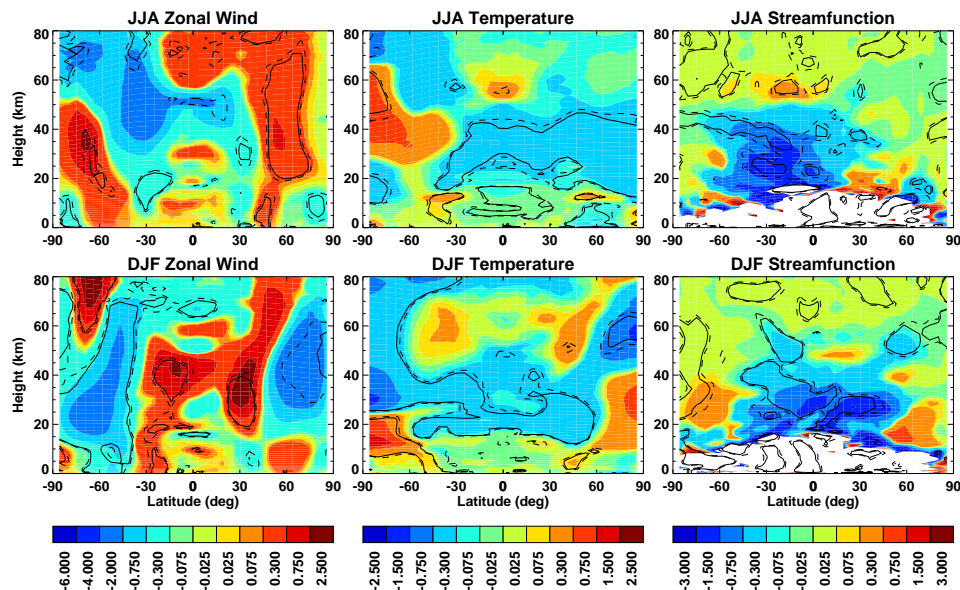


Fig. 13. June–August run mean, ensemble mean (top) and December–February run mean, ensemble mean (bottom) zonal wind (m/s), temperature (K), and mass streamfunction (kg/m², values outside the range (−4.4) not plotted) differences for the solar variability combined with EPP ensemble run compared to the solar variability only ensemble run.

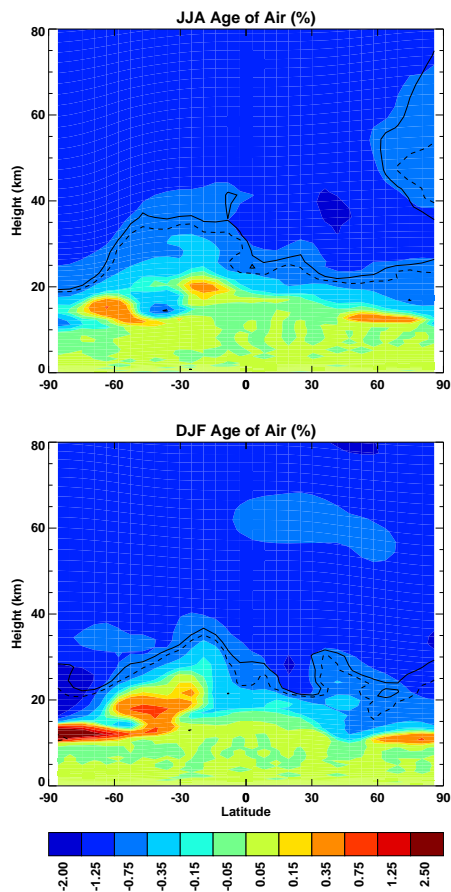


Fig. 14. Run mean, ensemble mean age of air (%) difference between the two ensembles shown in Fig. 13.

EPP impact on the middle atmosphere

K. Semeniuk et al.

Title Page

Abstract Introduction

Conclusions References

Tables Figures

◀ ▶

◀ ▶

Back Close

Full Screen / Esc

Printer-friendly Version

Interactive Discussion



EPP impact on the middle atmosphere

K. Semeniuk et al.

Title Page

Abstract

Introduction

Conclusions

References

Tables

Figures

◀

▶

◀

▶

Back

Close

Full Screen / Esc

Printer-friendly Version

Interactive Discussion

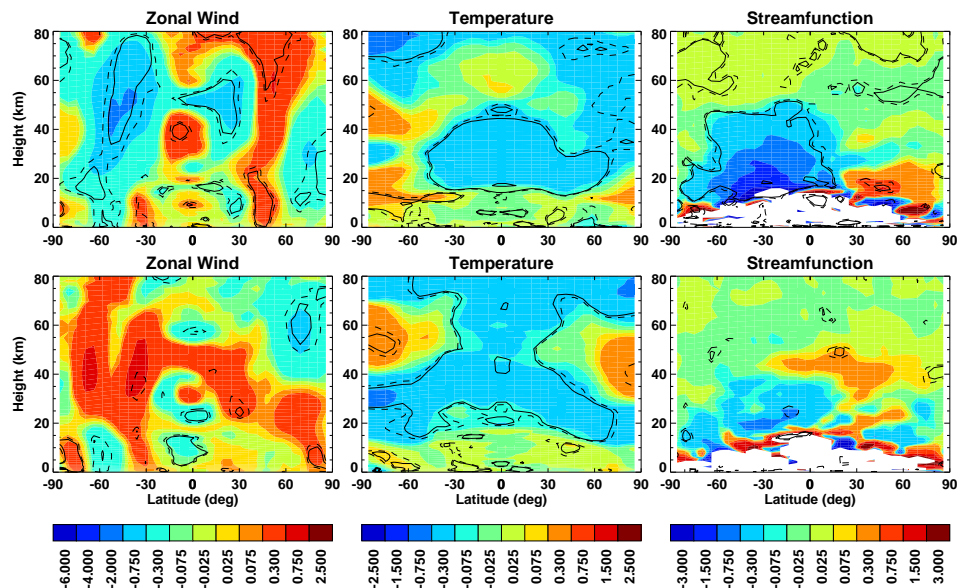


Fig. 15. Comparison of run mean, ensemble mean, annual mean difference from the reference ensembles of zonal wind (m/s) (left), temperature (K) (middle) and mass streamfunction (kg/m/s) (right). Top panels are for solar variability with EPP vs. solar variability only ensemble. Bottom panels are for the EPP without solar variability vs. the no EPP and no solar variability reference ensemble.

EPP impact on the middle atmosphere

K. Semeniuk et al.

Title Page

Abstract

Introduction

Conclusions

References

Tables

Figures

◀

▶

◀

▶

Back

Close

Full Screen / Esc

Printer-friendly Version

Interactive Discussion

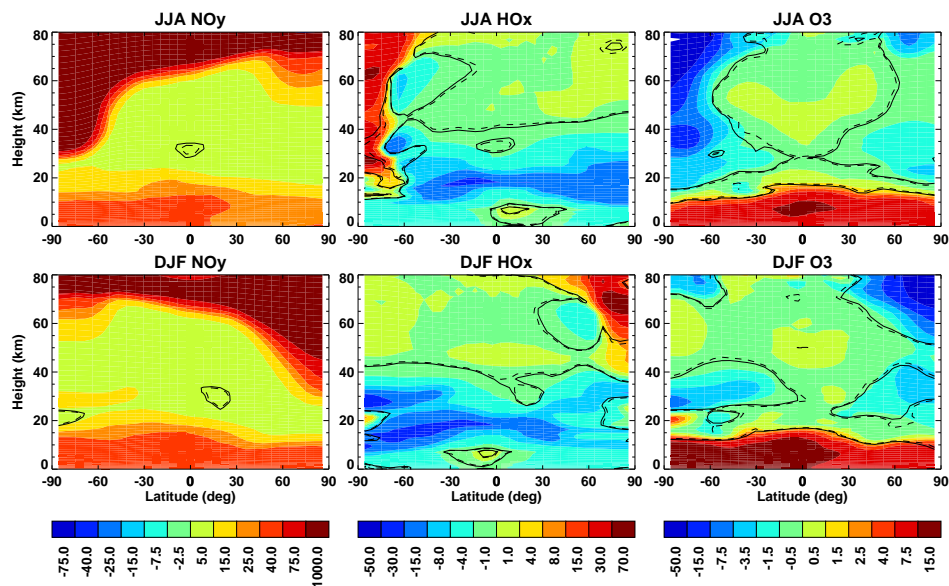


Fig. 16. Run mean, ensemble mean NO_y, HO_x and O₃ differences (%) between the two ensembles shown in Fig. 13.

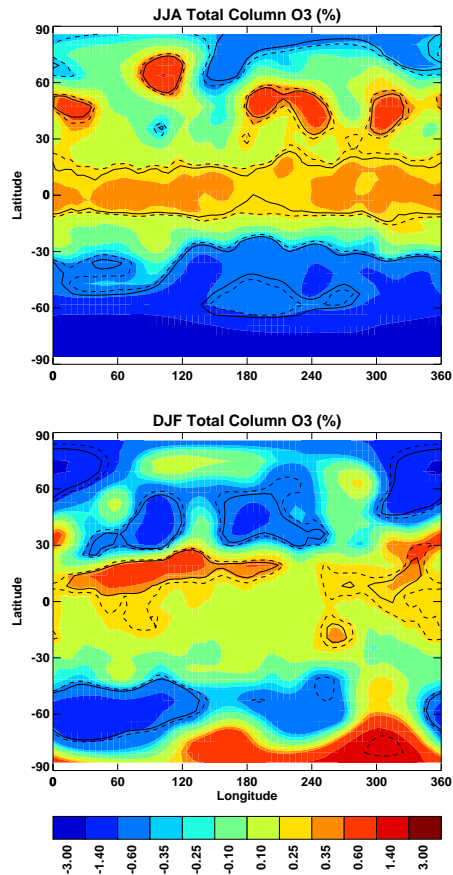


Fig. 17. Run mean, ensemble mean total column ozone (%) difference between the two ensembles shown in Fig. 13.

EPP impact on the middle atmosphere

K. Semeniuk et al.

Title Page

Abstract Introduction

Conclusions References

Tables Figures

◀ ▶

◀ ▶

Back Close

Full Screen / Esc

Printer-friendly Version

Interactive Discussion



EPP impact on the middle atmosphere

K. Semeniuk et al.

Title Page

Abstract

Introduction

Conclusions

References

Tables

Figures

◀

▶

◀

▶

Back

Close

Full Screen / Esc

Printer-friendly Version

Interactive Discussion

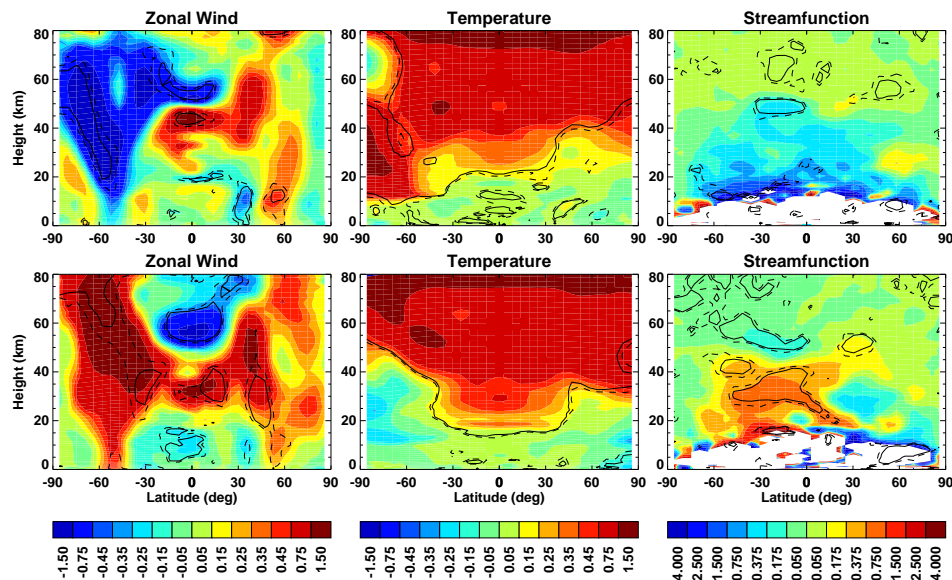


Fig. 18. Latitude-altitude regression coefficient for the solar variability only ensemble mean (top) and for the combined solar variability and EPP ensemble mean (bottom): (per 100 units of F10.7) left, zonal mean wind (m/s), middle, zonal mean temperature (K per 100 units F10.7), and right, mass streamfunction (kg/m/s, values outside the range (-5.5) are not plotted).

EPP impact on the middle atmosphere

K. Semeniuk et al.

Title Page

Abstract

Introduction

Conclusions

References

Tables

Figures

◀

▶

◀

▶

Back

Close

Full Screen / Esc

Printer-friendly Version

Interactive Discussion

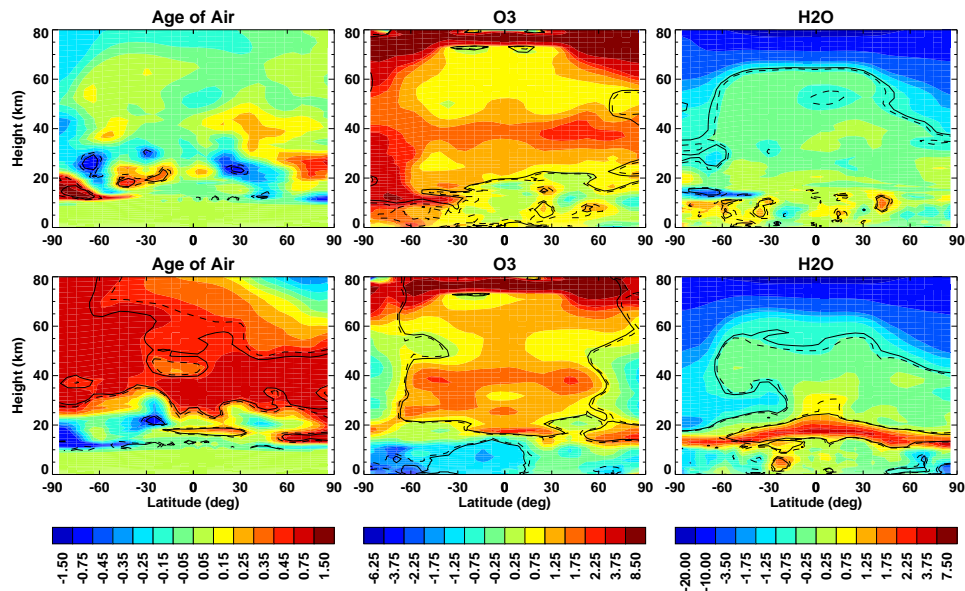


Fig. 19. As in Fig. 18 but for age of air (left), O₃ (middle), and H₂O (right). Differences in %.

EPP impact on the middle atmosphere

K. Semeniuk et al.

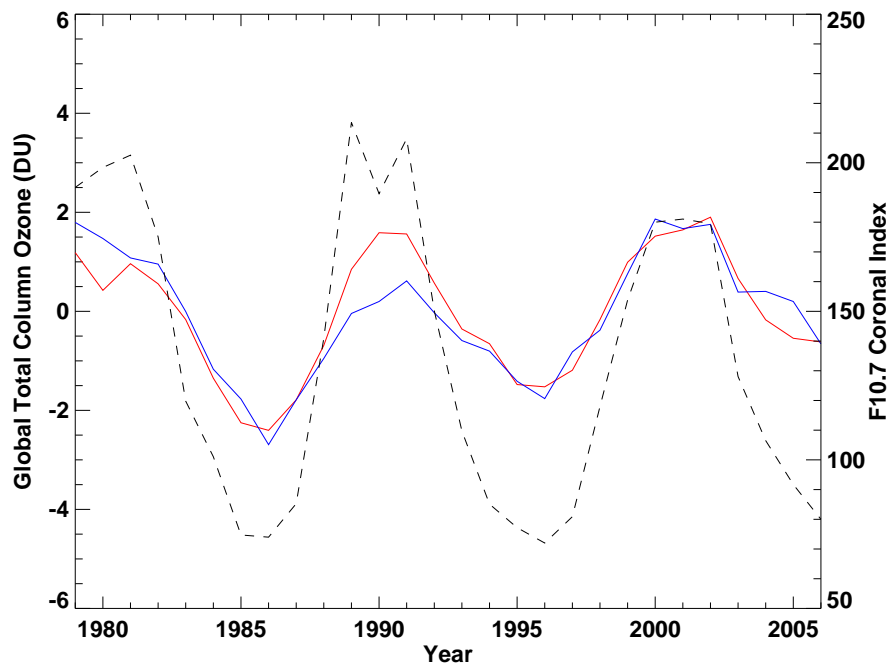


Fig. 20. Annual mean, global mean timeseries of the total column O_3 regression fit consisting of the F10.7 index term and the residual term for the solar variability ensemble without EPP (red) and the solar variability ensemble with EPP (blue). The F10.7 index is also shown (dashed).

[Title Page](#)[Abstract](#)[Introduction](#)[Conclusions](#)[References](#)[Tables](#)[Figures](#)[I◀](#)[▶I](#)[◀](#)[▶](#)[Back](#)[Close](#)[Full Screen / Esc](#)[Printer-friendly Version](#)[Interactive Discussion](#)

EPP impact on the middle atmosphere

K. Semeniuk et al.

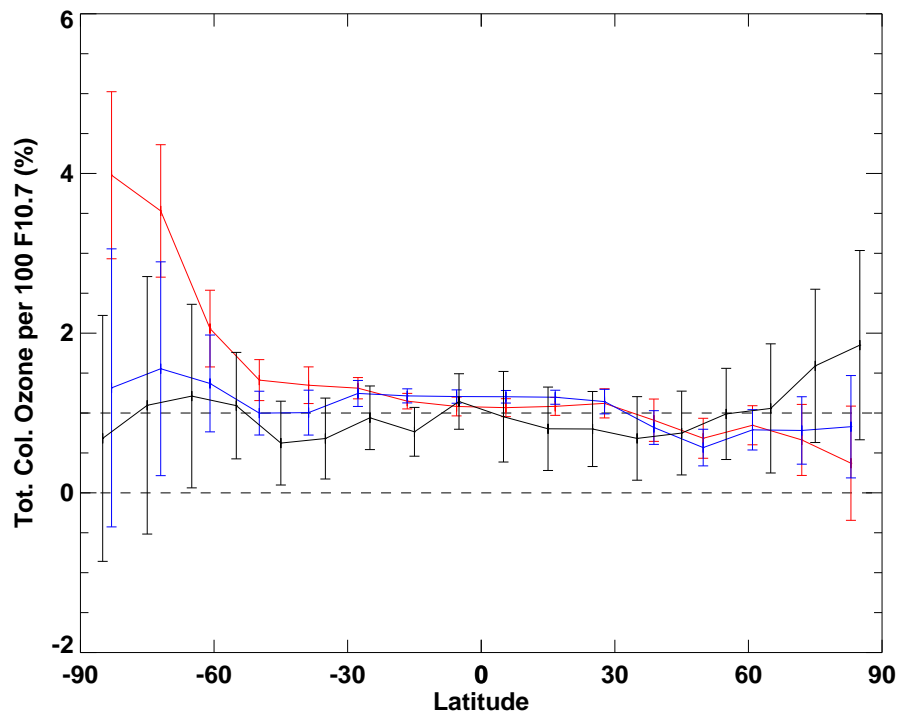


Fig. 21. Zonal mean total column O_3 regression fit against the F10.7 index for the ensemble without EPP (red) and the ensemble with EPP (blue). Regression of observed total column ozone from Fioletov et al. (2002) is also shown (black). The column O_3 response is in % per 100 units of F10.7. Error bars are $\pm 2\sigma$. The two dashed lines show the 0% and 1% levels.

[Title Page](#)[Abstract](#)[Introduction](#)[Conclusions](#)[References](#)[Tables](#)[Figures](#)[◀](#)[▶](#)[◀](#)[▶](#)[Back](#)[Close](#)[Full Screen / Esc](#)[Printer-friendly Version](#)[Interactive Discussion](#)

EPP impact on the middle atmosphere

K. Semeniuk et al.

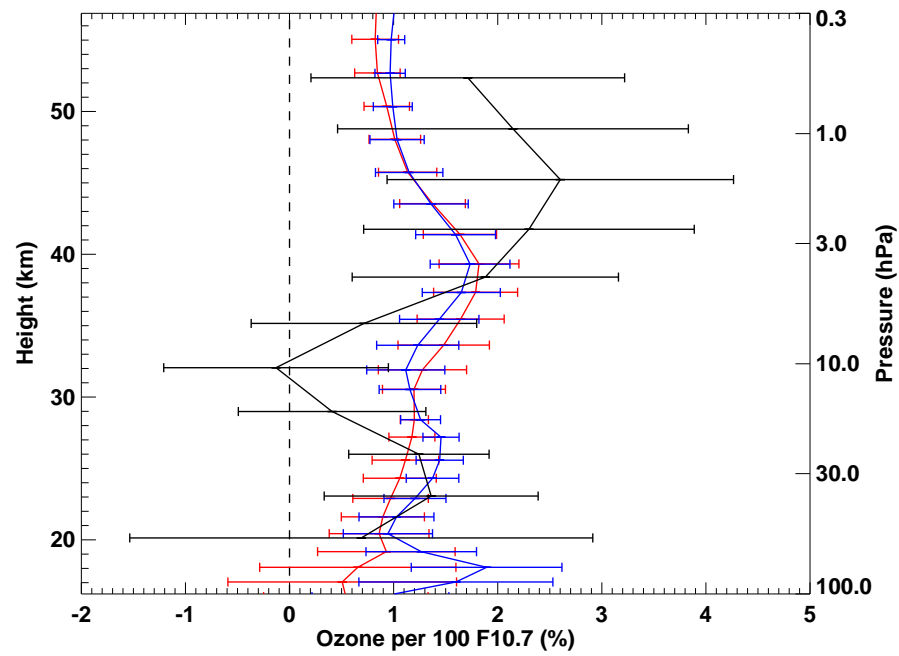


Fig. 22. Tropical mean, 25° S–25° N, O₃ regression coefficient for the ensemble without EPP (red) and the ensemble with EPP (blue). Regression of observed ozone (SAGE corrected SBUV, McLinden et al., 2009) is also shown (black). The O₃ response is in % per 100 units of F10.7. Error bars are $\pm 2\sigma$.

Title Page

Abstract

Introduction

Conclusions

References

Tables

Figures

◀

▶

◀

▶

Back

Close

Full Screen / Esc

Printer-friendly Version

Interactive Discussion



EPP impact on the middle atmosphere

K. Semeniuk et al.

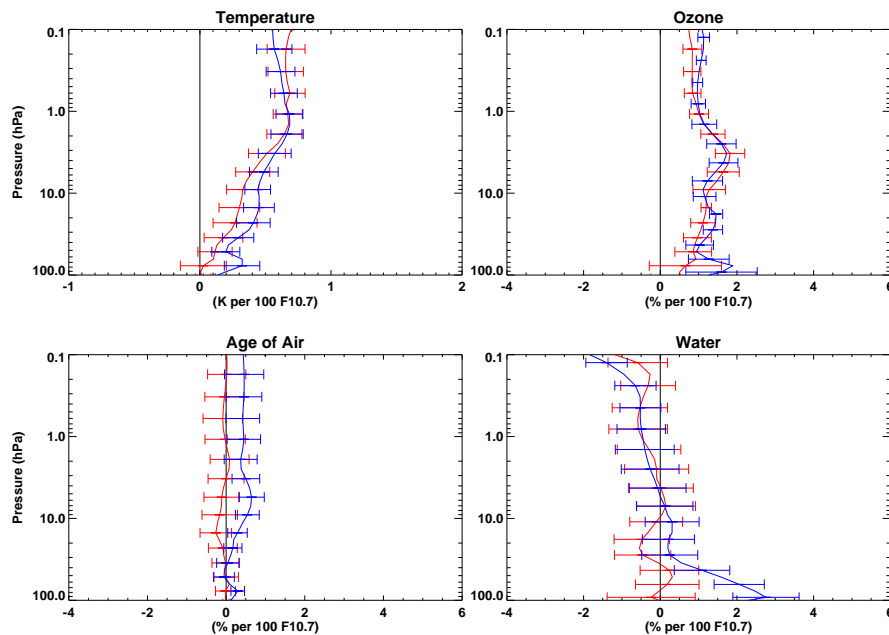


Fig. 23. Tropical mean, 25° S–25° N, temperature, ozone, age of air and water vapour regression fits for the ensemble without EPP (red) and the ensemble with EPP (blue). Error bars are $\pm 2\sigma$.

Title Page

Abstract

Introduction

Conclusions

References

Tables

Figures

◀

▶

◀

▶

Back

Close

Full Screen / Esc

Printer-friendly Version

Interactive Discussion

